

# Quantum stick-slip motion in nanoscaled friction

Dai-Nam Le<sup>1,\*</sup>, Pablo Rodriguez-Lopez<sup>2,†</sup> and Lilia M. Woods<sup>1,‡</sup>

<sup>1</sup>*Department of Physics, University of South Florida, Tampa, Florida 33620, USA*

<sup>2</sup>*Área de Electromagnetismo and Grupo Interdisciplinar de Sistemas Complejos (GISC),  
Universidad Rey Juan Carlos, 28933, Móstoles, Madrid, Spain*

(Dated: February 21, 2025)

Friction in atomistic systems is usually described by the classical Prandtl-Tomlinson model suitable for capturing the dragging force of a nanoparticle in a periodic potential. Here we consider the quantum mechanical version of this model in which the dissipation is facilitated by releasing heat to an external bath reservoir. The time evolution of the system is captured with the Liouville-von Neumann equation through the density matrix of the system in the Markov approximation. We examine several kinetic and dissipative properties of the nanoparticle by delineating classical vs quantum mechanical effects. We find that the Landau-Zener tunneling is a key factor in the overall reduction of the frictional dissipation when compared to the classical motion in which such tunneling is absent. This in-depth study analyzes the interplay between velocity, strength of interaction, and temperature to control the frictional process and provide useful guidelines for experimental data interpretation.

## I. INTRODUCTION

The relative motion between objects in close contact causes friction as a result of energy dissipated in this dynamical process. Friction often leads to reduced efficiency and reliability of machines and devices. Although friction has been extensively studied, the governing mechanisms are not completely understood yet [1, 2]. Computational studies using first principles methods have examined adhesion, corrugation, and van der Waals interaction energies for various materials [3–5] [another]. These directly related to static friction properties are instrumental in identifying materials with targeted tribological applications [6, 7].

The dynamical side of frictional processes is important in force microscopy applications [8] and typically, it is studied with continuum approaches that are variations of the Prandtl-Tomlinson model [9, 10]. This is essentially a classical approach in which a moving particle without internal degrees of freedom experiences stick-slip motion above a molecular chain represented as an oscillatory-like periodic potential. The dynamics of the process is modeled semi-empirically with materials-dependent parameters for the corrugation, velocity, and particle-chain interaction. The dynamical frictional properties of atomic/molecular chains in relative motion have also been studied within the Frenkel-Kontorova model [11–13], which was also used to understand dislocations, nonlinear effects and topological defects in relative chain displacements. Numerical methods, such as path integrals and quantum Monte Carlo simulations have shown the role of quantum and thermal fluctuations of the forced motion of an atom above a finite discrete chain. However, many-body collective phenomena at the quantum mechanical level are difficult to access via such algorithms due to numerical limitations associated with the size of the studied system.

A basic quantum mechanical effect important for the dynamics of frictional motion is the mixing between the energy states of the system creating conditions for tunneling. This is captured by the most basic assumptions in the Landau-Zener (LZ) theory [14, 15] in which the energy difference between two adiabatic states is violated by creating avoided level crossings. The LZ theory has found applications in dissipative and multilevel systems [16–18]. Curiously, a dissipative LZ two level system coupled to a bath of harmonic oscillator shows that the environmental temperature can actually enhance the probability of the system remaining in its ground state leading to quantum annealing [19].

In this paper, we investigate the quantum mechanical Prandtl-Tomlinson model in the presence of an external bath reservoir into which heat is released in the frictional dissipation. Several energetic, kinetic, and dissipative properties are defined and examined by using the density matrix of the Liouville-von Neumann equation in the Markov approximation. To better understand the quantum mechanical nature of the motion, we also investigate the quantum mechanical Prandtl-Tomlinson model in the absence of an external bath as well as the classical limit with and without an external bath using the stochastic Newton law. The released power and lateral force, in particular, give a quantitative representation of the frictional process and can be directly associated with experimental measurements.

---

\* [dainamle@usf.edu](mailto:dainamle@usf.edu); Homepage: <https://sites.google.com/view/dai-nam-le/>.

† [pablo.ropez@urjc.es](mailto:pablo.ropez@urjc.es)

‡ [lmwoods@usf.edu](mailto:lmwoods@usf.edu); Corresponding authors. Homepage: <https://www.amd-woods-group.com/>.

## II. MODEL SYSTEM

The system under consideration consists of a nanoscaled particle with mass  $M$  at a distance  $d$  above a one-dimensional infinitely long atomic chain with lattice period  $a$ , as shown in Fig. 1. The particle moves with a constant velocity  $v$  parallel to the chain. To maintain this motion, it is assumed that  $M$  is in an optical trap modeled by a harmonic potential. The particle also experiences the influence of a short-ranged interaction from the overlap of its atomic orbitals and the atomic orbitals of the chain. Additionally, there is a long-ranged van der Waals coupling originating from the exchange of electromagnetic fluctuations between  $M$  and the chain. The optical trap balances these different interactions by maintaining a motion parallel to the chain at a constant velocity.

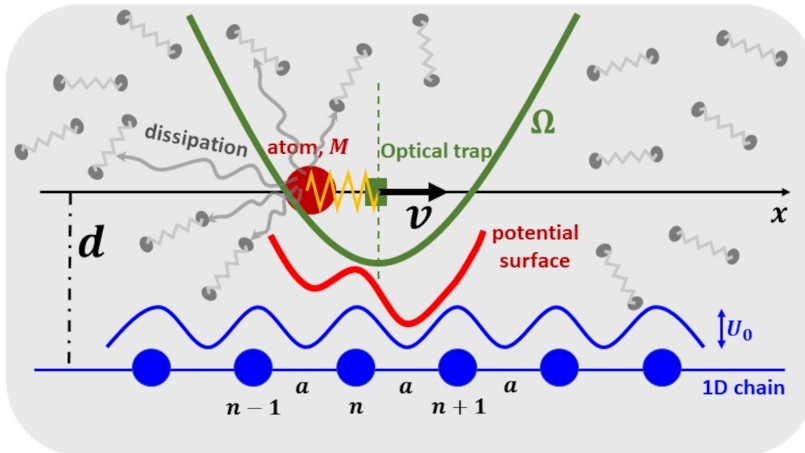


FIG. 1. Schematics of a particle with mass  $M$  confined in a harmonic potential moving with a constant velocity  $v$  above an infinitely long atomic chain with periodicity  $a$ . The distance  $d$  between the particle and the chain is maintained throughout the motion.

This system can be modeled by a 1D Hamiltonian given as

$$\hat{H}_S(t) = \frac{1}{2M}\hat{p}^2 + \frac{1}{2}M\Omega^2(x - vt)^2 + U_0(d)\sin^2\left(\frac{\pi x}{a}\right) + \Delta_0(d), \quad (1)$$

where the first term denotes the kinetic energy of the particle with its momentum operator  $\hat{p}$ . The second term contains a time-dependent harmonic term with a spring constant  $M\Omega^2$  associated with the moving optical trap of the nanoparticle ( $\Omega$  is a characteristic frequency). The spatial periodic term and the constant  $\Delta_0(d)$  reflect the combined effect of short-ranged interatomic and long-ranged van der Waals interactions. Assuming that  $d \gg a$ , one finds that  $U_0(d) = A_s\sqrt{\frac{2\pi dd_s}{a^2}}e^{-\frac{d}{d_s} - \frac{2\pi^2 dd_c}{a^2}} - \frac{3\pi C_6}{8ad^2}e^{-\frac{2\pi d}{a}}$  and  $\Delta_0(d) = \left[A_s\sqrt{\frac{2\pi dd_s}{a^2}}e^{-\frac{d}{d_s} - \frac{2\pi^2 dd_c}{a^2}} - \frac{3\pi C_6}{8ad^2}\right] - \frac{1}{2}U_0(d)$ . Here  $d_s$  and  $A_s$  are the decay length and magnitude of the short-range interaction, while  $C_6$  is the Hamaker constant following the Born-Mayer-Buckingham interatomic potential  $A_s e^{-r/d_s} - C_6 r^{-6}$  [20] (see section S-I in the Supplementary Information [21] for details). For a fixed distance  $d$ , the quantity  $\Delta_0(d)$  is simply a constant and can be dropped out from the above Hamiltonian since it only results in a global shift of the energy spectrum with no other consequences to the physics of the problem. The center of the driving optical trap is  $x_c = vt$ .

The above Hamiltonian can be re-written in a more convenient form,

$$\hat{H}_S(t) = -\frac{1}{2}\frac{\partial^2}{\partial \bar{x}^2} + \frac{1}{2}(\bar{x} - \bar{v}\bar{t})^2 + u_0 \sin^2\left(\frac{\pi \ell \bar{x}}{a}\right), \quad (2)$$

where  $u_0 = \frac{U_0(d)}{\hbar\Omega}$ ,  $\bar{x} = \frac{x}{\ell}$ ,  $\bar{t} = \frac{t}{\tau}$  and  $\bar{v} = \frac{v}{\nu}$  are unitless quantities expressed in terms of a characteristic length  $\ell = \sqrt{\frac{\hbar}{M\Omega}}$ , period of motion  $\tau = \frac{1}{\Omega}$ , and characteristic velocity  $\nu = \frac{\ell}{\tau} = \sqrt{\frac{\hbar\Omega}{M}}$ . This rescaling is equivalent to setting  $\hbar = M = \Omega = 1$ .

The above Hamiltonian is a quantum mechanical version of the classical Prandtl-Tomlinson model of a particle driven by a spring above a sinusoidally corrugated potential. This model has found many applications in the analysis of dynamic friction, especially in the understanding of experiments using atomic force microscopes [22]. It has also been utilized in capturing temperature in sliding frictional processes [23]. Nevertheless, this is a classical approach, and here we expand its applicability at the quantum mechanical level.



### A. Dynamics of the moving quantum particle: unitary evolution

To investigate the dynamical evolution of this closed system, we first solve the eigenvalue problem of the Schrödinger equation,

$$\hat{H}_S(\bar{t}) |n(\bar{t})\rangle = E_n(\bar{t}) |n(\bar{t})\rangle. \quad (3)$$

For this purpose, the eigenstates  $|n(\bar{t})\rangle$  are represented in terms of the eigenfunctions of a one-dimensional harmonic oscillator with a time-dependent displacement  $|n^{(0)}(\bar{t})\rangle = \frac{e^{-(\bar{x}-\bar{v}\bar{t})^2/2}}{\sqrt{2^n n! \sqrt{\pi}}} H_n(\bar{x} - \bar{v}\bar{t})$  where  $H_p$  are  $p$ -th Hermite polynomials [24]. The eigenstates are then decomposed as  $|n(\bar{t})\rangle = \sum_{p=0}^{\infty} c_{n,p}(\bar{t}) |p^{(0)}(\bar{t})\rangle$  with  $\sum_{p=0}^{\infty} |c_{n,p}(\bar{t})|^2 = 1$ . In this representation, Eq. (3) becomes the following eigenvalue equation in a matrix form,

$$\sum_{p'=0}^{\infty} (H_S)_{p,p'}(\bar{t}) c_{n,p'}(\bar{t}) = E_n(\bar{t}) c_{n,p}(\bar{t}). \quad (4)$$

The Hamiltonian matrix elements  $(H_S)_{n,n'}$  are found as

$$(H_S)_{n,n'}(\bar{t}) = \langle n^{(0)}(\bar{t}) | \hat{H}_S(t) | n'^{(0)}(\bar{t}) \rangle = \left( n + \frac{1}{2} + \frac{1}{2} u_0 \right) \delta_{n,n'} + u_0 \mathcal{V}_{n,n'}(\bar{t}). \quad (5)$$

$$\begin{aligned} \mathcal{V}_{n,n'}(\bar{t}) = \frac{(-1)^{\lfloor \frac{|n-n'|}{2} \rfloor}}{\sqrt{2^{|n-n'|+2}}} \sqrt{\frac{\min(n,n')!}{\max(n,n')!}} \left( \frac{2\pi\ell}{a} \right)^{|n-n'|} e^{-\frac{1}{4} \left( \frac{2\pi\ell}{a} \right)^2} \mathcal{L}_{\min(n,n')}^{|n-n'|} \left[ \frac{1}{2} \left( \frac{2\pi\ell}{a} \right)^2 \right] \\ \times \begin{cases} + \sin \left( \frac{2\pi\ell}{a} \bar{v}\bar{t} \right) & \text{when } |n-n'| \text{ is odd} \\ - \cos \left( \frac{2\pi\ell}{a} \bar{v}\bar{t} \right) & \text{when } |n-n'| \text{ is even} \end{cases}, \quad (6) \end{aligned}$$

where  $\mathcal{L}_a^b(x)$  are the associated Laguerre polynomials. Note that in this basis representation, the Hamiltonian matrix is given in an entirely analytical form. Its diagonal elements contain the time-independent eigenenergies of a harmonic oscillator shifted by a constant value. The time evolution is captured in the matrix element  $\mathcal{V}_{n,n'}(\bar{t})$  containing a decaying oscillatory-like functions with period  $a/\ell$ . See in section S-II in the Supplementary Information [21] for derivation of these matrix elements.

Eqs.(4)-(6) can now be solved numerically to find the time-dependent eigenvalues  $E_n(\bar{t})$  of the Hamiltonian of the system with corresponding eigenvectors labeled as  $[c_{n,0}(\bar{t}), c_{n,1}(\bar{t}), c_{n,2}(\bar{t}), \dots]^T$ . The infinite dimension of the Hamiltonian matrix is problematic for the numerical calculations, thus restrictions to a large enough matrix are imposed. As we focus on the lowest five eigenenergies, the eigenvalue problem is solved for an  $H_S$  matrix with 25 elements, which is sufficiently large enough for convergence. More details about the diagonalization of  $\hat{H}_S$  and the numerical procedure can be found in section S-III in the Supplementary Information [21].

The dynamical evolution of this closed system can be described by the density matrix operator  $\hat{\rho}_S(\bar{t})$  governed by the Liouville-von Neumann equation [25]. Utilizing the basis set of the time-dependent harmonic oscillator  $|n^{(0)}(\bar{t})\rangle$ , this equation can be cast into

$$\frac{d}{d\bar{t}} \rho_S(\bar{t}) = -i [H_S(\bar{t}) - \sigma_t(\bar{t}), \rho_S(\bar{t})], \quad (7)$$

with matrix elements  $(\rho_S)_{n,n'}(\bar{t}) = \langle n^{(0)}(\bar{t}) | \hat{\rho}_S(\bar{t}) | n'^{(0)}(\bar{t}) \rangle$  and  $(\sigma_t)_{n,n'}(\bar{t}) = i \langle n^{(0)}(\bar{t}) | \left( \frac{d}{d\bar{t}} | n'^{(0)}(\bar{t}) \rangle \right)$ . The explicit expression of the Hermitian matrix  $(\sigma_t)_{n,n'}(\bar{t})$  is given in section S-IV in the Supplementary Information [21]. To solve the above equation, we utilize forth-order Runge-Kutta method [26].

The evolution of this system is studied by tracking several properties defined with the density matrix operator. These include the instantaneous average energy of the system  $\langle E \rangle(\bar{t})$ , the eigenstate population  $P_n(\bar{t})$ , and linear entropy  $S_L(\bar{t})$  conveniently defined in Table I. As  $\langle E \rangle$  changes in time,  $P_n(\bar{t})$  shows the different eigenstate contributions in the dynamical state of the moving particle at each point in time. Also,  $S_L(\bar{t})$  measures the states mixture as a function of time [27]. We can also track the time-dependent global geometric phase of the system determined as [28],

$$\gamma(\bar{t}) = \arg \left[ \sum_k \sqrt{\xi_k(0)\xi_k(\bar{t})} \langle \phi_k(0) | \phi_k(\bar{t}) \rangle \exp \left( - \int_0^{\bar{t}} \langle \phi_k(0) | \frac{d\phi_k}{d\bar{t}}(\bar{t}) \rangle d\bar{t} \right) \right]. \quad (8)$$

where  $\xi_k(\bar{t})$  and  $|\phi_k(\bar{t})\rangle$  are instantaneous eigenvalues and associated eigenvectors of the density matrix operator, such that  $\hat{\rho}_S = \sum_k \xi_k(\bar{t}) |\phi_k(\bar{t})\rangle \langle \phi_k(\bar{t})|$ . The quantity  $\gamma(\bar{t})$  is exclusively associated with the geometric path of the quantum mechanical state in time.

TABLE I. Quantum mechanical properties of the coupled moving particle/atomic chain system. Here the linear entropy is renormalized by a factor  $\frac{N_{max}}{N_{max}-1}$  where  $N_{max}$  is the cutoff size of the Hamiltonian as suggested in Ref. [27]. The standard deviation of an arbitrary observable  $\hat{a}$  is  $\sigma_a = \sqrt{\text{Tr}[\hat{a}^2 \hat{\rho}_S(\bar{t})] - \text{Tr}[\hat{a} \hat{\rho}_S(\bar{t})]^2}$ . The work associated with the moving harmonic trap  $\mathcal{W}(\bar{t})$  is calculated from the following integral  $\mathcal{W}(\bar{t}) = \int_0^{\bar{t}} \text{Tr}[\hat{\rho}_S(\bar{t}') \frac{d\hat{H}_S(\bar{t}')}{d\bar{t}'}] d\bar{t}'$ .

Internal properties	Kinematic properties	Dynamic properties
Average energy $\langle E \rangle(\bar{t}) = \text{Tr}[\hat{\rho}_S(\bar{t}) \hat{H}_S(\bar{t})]$	Average position $\langle x \rangle(\bar{t}) = \text{Tr}[\hat{x} \hat{\rho}_S(\bar{t})]$	Heat transfer $Q = \Delta \langle E \rangle(\bar{t}) - \mathcal{W}(\bar{t})$
Eigenstate population $P_n(\bar{t}) = \langle n(\bar{t})   \hat{\rho}_S(\bar{t})   n(\bar{t}) \rangle$	Average velocity $\langle v \rangle(\bar{t}) = M^{-1} \text{Tr}[\hat{p} \hat{\rho}_S(\bar{t})]$	Power transfer $P = Q/\bar{t}$
Linear entropy $S_L(\bar{t}) = \frac{N_{max}}{N_{max}-1} (1 - \text{Tr}[\hat{\rho}_S^2])$	Heisenberg Principle $\sigma_x(\bar{t}) \sigma_p(\bar{t})$	Lateral force $\langle F_L \rangle(\bar{t}) = -M\Omega^2 (\bar{x}(\bar{t}) - \bar{v}\bar{t})$
Geometric phase $\gamma(\bar{t})$ as in Eq. (8)		

Before presenting results from the numerical calculations, we examine some limiting cases as dictated by the properties of the Hamiltonian. Eqs. (5), (6) show that the characteristic behavior of the matrix elements  $\mathcal{V}_{n,n}(\bar{t})$  is controlled by the parameters  $\frac{2\pi\ell}{a}$  and the velocity  $\bar{v} = \frac{v}{\nu}$ . In the case of  $a \ll \ell$ , the asymptotic behavior of the exponential term  $e^{-\frac{1}{4}(\frac{2\pi\ell}{a})^2} \rightarrow 0$  makes the last term in the Hamiltonian matrix (5) negligible. Consequently, the eigenenergies of the system are simply the diagonal elements of  $H_S$ :  $E_n(\bar{t}) \approx n + \frac{1}{2} + \frac{u_0}{2}$ . This is understood by realizing that the optical trap “sees” an almost continuous chain due to the very small  $a$ , thus the particle effectively behaves as a shifted harmonic trap with constant eigenenergies.

In the case of  $a \gg \ell$ , the  $\mathcal{V}_{n,n}(\bar{t})$  off-diagonal elements diminish since  $\left(\frac{2\pi\ell}{a}\right)^{|n-n'|} \rightarrow 0$  and only the diagonal terms matter. As a result, the eigenenergies become oscillatory according to  $E_n(\bar{t}) \approx n + \frac{1}{2} + \frac{u_0}{2} - \frac{u_0}{2} \cos\left(\frac{2\pi\ell}{a}\bar{v}\bar{t}\right)$ . This situation corresponds to the harmonic trap of the particle being much narrower than the periodic potential of the atomic chain. The particle is effectively trapped in the minimum of the potential as it moves along the chain. In both limits,  $\left(\frac{2\pi\ell}{a}\right) \rightarrow 0$  or  $\left(\frac{2\pi\ell}{a}\right) \rightarrow \infty$ , the gaps between the eigenenergies are time-independent.

When the ratio  $\left(\frac{2\pi\ell}{a}\right) \sim 1$ , however, the off-diagonal elements play a vital role for the particle as the eigenstates now experience the influence of different  $|n^{(0)}(\bar{t})\rangle$ . For example, it is possible that the potential of the system evolves from a harmonic trap with a single minimum to one with a double minima. This occurs when the depth of the periodic potential satisfies  $u_0 > 2\left(\frac{a}{2\pi\ell}\right)^2$ . As a result, there are anti-crossings between eigenenergy levels signaling the occurrence of Landau-Zener tunneling [14, 15] whose probability is also controlled by the velocity  $\bar{v}$ . One notes that the condition supporting Landau-Zener tunneling  $u_0 > 2\left(\frac{a}{2\pi\ell}\right)^2$  is consistent with the condition for the occurrence of stick-slip motion in the classical Prandtl-Tomlinson model [29–31] defined through the corrugation parameter  $\eta = \frac{u_0}{2}\left(\frac{2\pi\ell}{a}\right)^2 > 1$ . Unlike the classical Prandtl-Tomlinson model, multiple stick-slip motion requires constraints not only through the corrugation parameter  $\eta$  but also the ratio  $\left(\frac{2\pi\ell}{a}\right)$ . With a fixed corrugation parameter  $\eta$ , the shape of the potential surface of the particle at  $t = T/2$  is invariant but the ratio  $\left(\frac{2\pi\ell}{a}\right)$  controls the scale of that potential surface. As a known result from quantum mechanics for the double-well potential, the depth of the wells would tell us how many energy levels stay inside the wells and the numbers of the anti-crossing levels (see Ref. [32] for example). If there are no anti-crossing levels (when  $\left(\frac{2\pi\ell}{a}\right)$  is too large or too small), there is no Landau-Zener diabatic transition and consequently there is no stick-slip motion.

In Fig. 2(a-d), we show the evolution of the lowest five eigenenergies of the particle for different velocities together with their population dynamics in Fig. 2(e-h) by focusing on the Landau-Zener tunneling regime. For this purpose,

we take  $\frac{a}{2\pi\ell} = 1$  and  $u_0 = 5$ , which corresponds to a corrugation classical parameter  $\eta = 2.5 > 1$ . From the theory of Landau-Zener tunneling [14, 15], the probability of a diabatic transition at the anti-crossing between levels  $n$  and  $n'$  is estimated as  $P_{n \rightarrow n'} = \exp\left(-\frac{v_{n,n'}}{v}\right)$  where  $v_{n,n'} = \frac{\pi|E_n - E_{n'}|^2}{2\frac{\partial|E_n - E_{n'}|}{\partial x_c}}$  with  $x_c = vt$  being the position of the center of the optical trap. Thus for  $\frac{a}{2\pi\ell} = 1$  and  $u_0 = 5$ , we estimate that  $v_{01} = 8.39 \times 10^{-4}\nu$ ,  $v_{12} = 1.75 \times 10^{-2}\nu$ ,  $v_{23} = 1.25 \times 10^{-1}\nu$  and  $v_{34} = 4.50 \times 10^{-1}\nu$ .

By tracking  $\langle E \rangle(t)$  in Fig. 2a for  $v = 0.005\nu$ , we find that the particle starts out in the ground state of  $\hat{H}_S$ . At  $t/T = 0.5$  the anti-crossing between  $n = 0$  and  $n = 1$  states induces a diabatic tunneling transition with probability of  $P_{0 \rightarrow 1} \approx 85\%$  (Fig. 2e). Afterwards, the particle is in a superposition composed of the  $n = 0$  and  $n = 1$  states since higher-level transitions are negligible. The two states are disentangled by a diabatic transition from  $n = 1$  to  $n = 0$  at  $t/T = 1.5$ . Indeed, Fig. 2e shows that for  $t/T = (0.5, 1.5)$  the level population contains about 82 % from the first excited state and about 15 % from the ground state, while the remaining part belongs to the second excited state. In the interval  $t/T = (1.5, 2.5)$ , the population is composed of about 95 % contributions from the ground state and the diabatic transition at  $t/T = 2.5$  redistributes the populations with about 23 %, 70 % and 7 % for  $n = 0, 1, 2$  states.

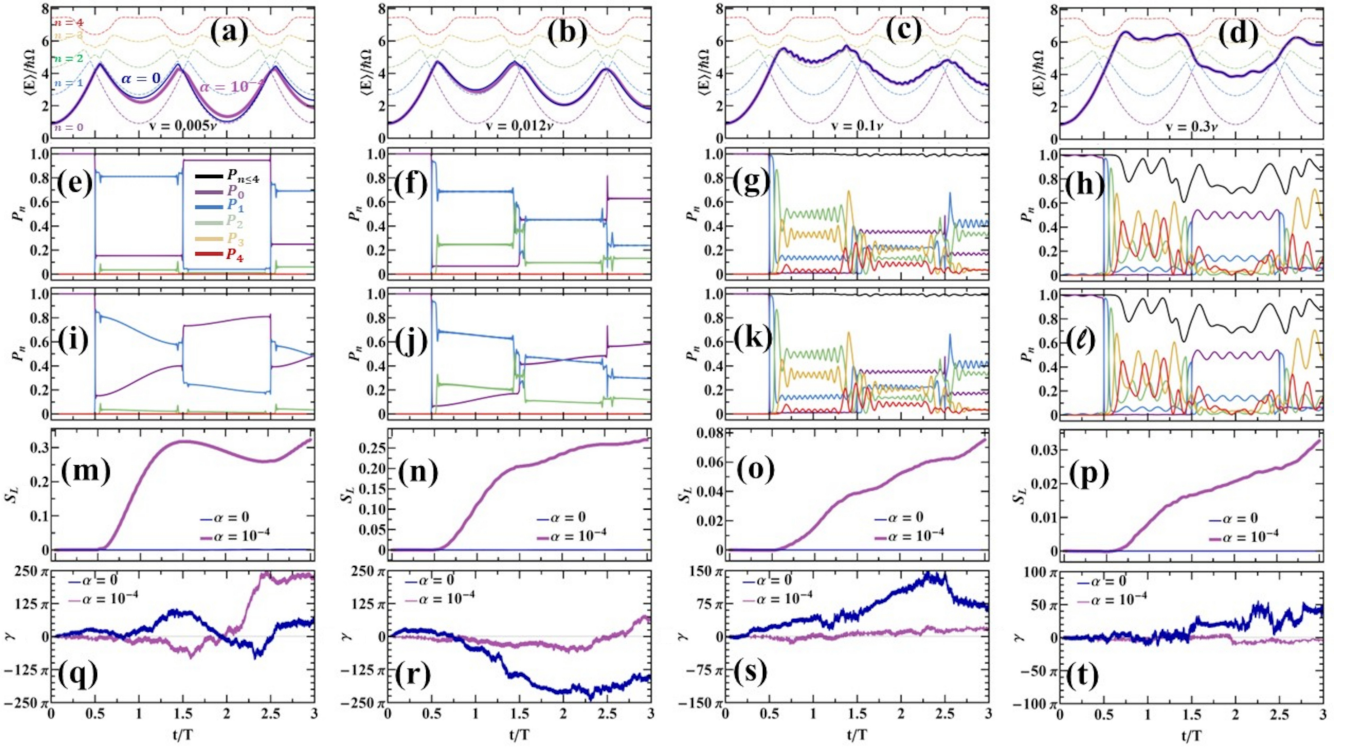


FIG. 2. The average energy  $\langle E \rangle$  and the first five eigenenergies of Hamiltonian  $\hat{H}_S(t)$  normalized by  $\hbar\Omega$  as a function of time rescaled by the period  $T = a/v$  for (a)  $v = 0.005\nu$ , (b)  $v = 0.012\nu$ , (c)  $v = 0.1\nu$  and (d)  $v = 0.3\nu$ . The population of the first five eigenstates of  $\hat{H}_S(t)$  as a function of time  $t/T$  for (e)  $v = 0.005\nu$ , (f)  $v = 0.012\nu$ , (g)  $v = 0.1\nu$  and (h)  $v = 0.3\nu$ . The population of the first five eigenstates of  $\hat{H}(t)$  as a function of time  $t/T$  for (i)  $v = 0.005\nu$ , (j)  $v = 0.012\nu$ , (k)  $v = 0.1\nu$  and (l)  $v = 0.3\nu$ . The linear entropy as a function of time  $t/T$  for  $\hat{H}_S(t)$  and  $\hat{H}(t)$  for (m)  $v = 0.005\nu$ , (n)  $v = 0.012\nu$ , (o)  $v = 0.1\nu$  and (p)  $v = 0.3\nu$ . The geometric phase as a function of time  $t/T$  for  $\hat{H}_S(t)$  and  $\hat{H}(t)$  for (q)  $v = 0.005\nu$ , (r)  $v = 0.012\nu$ , (s)  $v = 0.1\nu$  and (t)  $v = 0.3\nu$ . Here the distance between the particle and the chain is  $a = 2\pi\ell$ , the depth of the periodic potential is  $U_0 = 5\hbar\Omega$ . The temperature and cutoff energy of the harmonic bath are  $k_B T = 0.01\hbar\Omega$ ,  $\hbar\omega_c = 50\hbar\Omega$ , and the particle-bath coupling constant in  $\hat{H}(t)$  is taken as  $\alpha = 10^{-4}$ .

Increasing the velocity to  $v = 0.012\nu$  activates tunneling between  $n = 0 \rightarrow n = 1$  and  $n = 1 \rightarrow n = 2$  at  $t/T \sim 0.5$  and between  $n = 2 \rightarrow n = 3$  at  $t/T \approx 0.6$  with corresponding transition probabilities  $P_{0 \rightarrow 1} = 93\%$ ,  $P_{1 \rightarrow 2} = 23\%$  and  $P_{2 \rightarrow 3} = 0.003\%$ . As a result, there are various redistributions in the level populations, as shown in Fig. 2f. At  $v = 0.1\nu$  and  $v = 0.3\nu$  velocities, tunneling involving higher energetic states with increasing probabilities are further activated. Thus, the particle experiences the Landau-Zener tunneling effects from higher laying energy levels ((Fig. 2c,g) and Fig. 2d,h). This slow-to-fast moving particle progression shown in Fig. 2 is accompanied by transitioning

to more complicated time-dependent tunneling between higher states with complex patterns of periodicity.

## B. Dynamics of the moving quantum particle with coupling to the environment

The dynamics of the system described by the Hamiltonian in Eqs. (1)-(2) corresponds to a coherent evolution of a closed system and it exemplifies internal quantum mechanical effects in the motion. The forced motion of the particle, however, results in energy removed by dissipation. To model this we consider that the particle/atomic chain system is coupled to an external thermostat taken as a harmonic bath in the Caldeira–Leggett model [18, 33, 34]

$$\hat{H}(t) = \hat{H}_S(t) + \hat{H}_{int+B}, \quad \hat{H}_{int+B} = \sum_i \left[ -\frac{1}{2m_i} \frac{\partial^2}{\partial x_i^2} + \frac{1}{2} m_i \omega_i^2 \left( x_i - \frac{c_i}{m_i \omega_i^2} \sin \left( \frac{2\pi \ell}{a} \bar{x} \right) \right)^2 \right], \quad (9)$$

where  $x_i$  are the spatial degrees of freedom of the bath oscillation modes with parameters  $m_i, \omega_i, c_i$  for their mass, frequency, and strength, respectively. The bath is characterized by a spectral function  $J(\omega) = \sum_i \frac{c_i^2}{2m_i \omega_i} \delta(\omega - \omega_i)$  which describes the dissipative coupling with the system [34, 35]. Here we focus on the Ohmic dissipation limit with  $J(\omega) = 2\alpha\omega e^{-|\omega|/\omega_c}$ , where  $\omega_c$  is a cutoff frequency separating the low-frequency regime for which  $J(\omega) \propto \omega$  and the high-frequency regime specified by a decaying Ohmic damping. The dimensionless constant  $\alpha \ll 1$  specifies the coupling between the particle/chain system and the harmonic bath. Notice that if  $\alpha = 0$ , then  $J(\omega) = 0$  for all frequencies and  $c_i = 0$  i.e. there is no coupling between the system and the bath and  $\hat{H}_{int} = 0$ .

To continue further, the Hamiltonian in Eq. (9) is represented by separating the degrees of freedom of the nanoparticle from the degrees of freedom of the harmonic bath, such that

$$\hat{H}(t) = \hat{H}'_S(\bar{t}) \otimes \hat{1}_B + \hat{A} \otimes \hat{B} + \hat{1}_S \otimes \hat{H}_B, \quad (10)$$

with a renormalization operator  $\hat{A} = \sin \left( \frac{2\pi \ell}{a} \bar{x} \right)$  and  $\hat{H}'_S(\bar{t}) = \hat{H}_S(\bar{t}) + u_{rn} \hat{A}^2$  act in the subspace of the particle, while  $\hat{B} = -\sum_i c_i x_i$  and  $\hat{H}_B = \sum_i \left( -\frac{1}{2m_i} \frac{\partial^2}{\partial x_i^2} + \frac{1}{2} m_i \omega_i^2 x_i^2 \right)$  operate in the subspace of the harmonic bath. The term  $u_{rn} \hat{A}^2$  captures the dissipative coupling between the moving particle and the heat bath. The renormalization constant can be determined via the spectral density function  $u_{rn} = \sum_i \frac{c_i^2}{2m_i \omega_i^2} = \sum_i \frac{c_i^2}{2m_i \omega_i} \int_0^{+\infty} \omega_i^{-1} \delta(\omega - \omega_i) d\omega = \int_0^{+\infty} \omega^{-1} J(\omega) d\omega = 2\alpha\omega_c$ , as also shown in Ref.[18]. This renormalization potential in the total Hamiltonian (9) ensures that the system maintains its global minimum regardless of the bath [34].

Assuming weak coupling consistent with the Born-Markov approximation, the quantum Liouville - von Neumann master equation for the density matrix is written as [25]

$$\frac{d}{d\bar{t}} \hat{\rho}_S(\bar{t}) = -i \left[ \hat{H}'_S(\bar{t}) + 2\alpha\omega_c \hat{A}^2, \hat{\rho}_S(\bar{t}) \right] - \left\{ \left[ \hat{A}, \hat{S}(\bar{t}) \hat{\rho}_S(\bar{t}) \right] + \text{Hermitian conjugate} \right\}, \quad (11)$$

where the bath-convoluted operator  $\hat{S}(t)$  is defined as  $\hat{S}(t) \approx \sum_{m,n} \langle n(\bar{t}) | \hat{A} | m(\bar{t}) \rangle \Gamma(E_m - E_n) |n(\bar{t})\rangle \langle m(\bar{t})|$  in which the bath-induced transition rate  $\Gamma(E)$  is simply the Fourier transform of the bath correlation function  $C(\tau)$  for which  $\Gamma(E) = \int_0^{+\infty} d\tau C(\tau) e^{i(E+i0^+)\tau}$ . Taking into account that the harmonic bath is in a thermal equilibrium obeying Bose-Einstein distribution  $f_{BE}(\omega) = (e^{\omega/k_B T} - 1)^{-1}$ , the bath correlation function can be expressed in term of the spectral function  $C(\tau) = \int_{-\infty}^{+\infty} e^{i\omega\tau} f_{BE}(\omega) J(\omega) d\omega$ . The bath-induced transition rate can further be simplified as  $\Gamma(E) = \frac{1}{2} \gamma(E) + i\sigma(E)$  where  $\gamma(E) = \frac{4\pi\alpha E e^{-|E|/\omega_c}}{1 - e^{-|E|/k_B T}}$  and  $\sigma(E) = \mathcal{P} \int_{-\infty}^{+\infty} \frac{2\alpha\xi e^{-|\xi|/\omega_c} d\xi}{(E+\xi)(e^{-\xi/k_B T} - 1)}$ . For  $E = 0$ ,  $\gamma(0) = 4\pi\alpha k_B T$  and  $\sigma(0) = -2\alpha\omega_c$ .

Similar to the case of the moving particle with no external bath, Eq. (11) can be expressed in the basis set of the time-dependent harmonic oscillators  $|n^{(0)}(\bar{t})\rangle = \varphi_n^{HO}(\bar{x} - \bar{v}\bar{t})$ :

$$\frac{d}{d\bar{t}} \rho_S(\bar{t}) = -i \left[ H_S(t) + 2\alpha\omega_c A^2(\bar{t}) - \sigma_t(\bar{t}), \rho_S(\bar{t}) \right] - \left\{ [A(\bar{t}), S(\bar{t}) \rho_S(\bar{t})] + \text{Hermitian conjugate} \right\}, \quad (12)$$

where the matrix elements of  $\hat{A}$  and  $\hat{S}(\bar{t})$  are given as follows

$$\begin{aligned}
A_{n,n'}(\bar{t}) &= \left\langle n^{(0)}(\bar{t}) \left| \sin \left( \frac{2\pi\ell}{a} \bar{x} \right) \right| n'^{(0)}(\bar{t}) \right\rangle \\
&= \frac{(-1)^{\lfloor \frac{|n-n'|}{2} \rfloor}}{\sqrt{2^{|n-n'|+2}}} \sqrt{\frac{\min(n,n')!}{\max(n,n')!}} \left( \frac{2\pi\ell}{a} \right)^{|n-n'|} e^{-\frac{1}{4} \left( \frac{2\pi\ell}{a} \right)^2} \mathcal{L}_{\min(n,n')}^{|n-n'|} \left[ \frac{1}{2} \left( \frac{2\pi\ell}{a} \right)^2 \right] \\
&\quad \times \begin{cases} \cos \left( \frac{2\pi\ell}{a} \bar{v}\bar{t} \right) & \text{when } |n-n'| \text{ is odd} \\ \sin \left( \frac{2\pi\ell}{a} \bar{v}\bar{t} \right) & \text{when } |n-n'| \text{ is even} \end{cases}, \tag{13}
\end{aligned}$$

$$S_{n,n'}(\bar{t}) = \sum_{m,m',k,k'} c_{m,n}(\bar{t}) c_{m,k}^*(\bar{t}) A_{k,k'}(\bar{t}) c_{m',k'}(\bar{t}) c_{m',n'}^*(\bar{t}) \Gamma [E_{m'}(\bar{t}) - E_m(\bar{t})]. \tag{14}$$

Details about the derivation of  $\hat{H}(t)$  and the quantum Liouville-von Neumann equation are given in section S-V in the Supplementary Information [21].

The dynamic evolution of the particle is now examined based on Eqs. (10),(11) by turning on the coupling to the bath with parameters  $\alpha = 10^{-4}$ ,  $\omega_c = 50\Omega$  and  $k_B T = 0.01\hbar\Omega$ . Here, we choose  $\alpha$  small enough to maintain the validity of Born-Markov approximation, while  $\omega_c$  is large enough to include higher energy level transitions in the system.

In Fig.2 (a-d), we show the numerical calculations for the ground state average energy for the system/bath Hamiltonian. The  $\alpha = 0$  and  $\alpha = 10^{-4}$  results are very similar, especially for larger velocities. The role of the bath can be better discerned by looking at the level population dynamics. Fig. 2(i-l) shows that for  $t/T < 0.5$  the particle remains in its ground state for practically all studied velocities. At  $t/T \approx 0.5$  the particle experiences tunneling and it acquires higher level energy states. For the  $v = 0.005\nu$  case, for example, Fig. 2(i) shows that in the  $t/T = (0.5, 1.5)$  interval, the ground and excited state admixture changes in time in such a way that both contributions become of similar value at the end of the interval - 40% from the ground state and 60% for the first excited state. This type of admixture dynamics becomes more complex for higher velocities.

Clearly, the disorder in the system has increased after the initial tunneling at  $t/T \approx 0.5$  due to the coupling with the external bath. This correlates well with the linear entropy in Fig.2 (m-p), which shows that  $S_L$  increases over time when the system is coupled to the external thermostat, while  $S_L$  remains zero for the closed system.

Signatures of the Landau-Zener tunneling and coupling to the environment can also be found in the geometric phase, shown in Fig. 2(q-t). The different crossings involved in the dynamics of the system can cause a complex behavior of  $\gamma(\bar{t})$  leading to interference of transition path interference due to different phase accumulations [36]. Experimental interferometry measurements can access the Landau-Zener tunneling geometric phase in different atomic and optical systems [37, 38]. Fig. 2(q-t) shows that for the unitary evolution of the system,  $\gamma(\bar{t})$  is strongly dependent on the velocity of the particle. The geometric phase experiences different behavior in time and it can even change sign. Turning on the coupling to the bath adds dissipation which further adds to the complexity of  $\gamma$ . Nonunitary effects have been studied in various two-level systems [39–41] demonstrating that  $\gamma$  has a stochastic character due to occurring random quantum phase jumps. Fig. 2(q-t) further shows that the frictional dissipation has significant influence on the geometric phase of the particle for each studied velocity adding to the complex behavior of  $\gamma(\bar{t})$ .

### C. Dynamics of the moving particle within the classical Prandtl-Tomlinson model

In order to understand better the quantum mechanical effects in the frictional dissipation process, we also examine the motion of the particle within the classical Prandtl-Tomlinson model. From the classical version of the Hamiltonian in (9), the stochastic dynamics of the particle is captured through the Hamilton's equations of motion with coupling to an external bath via a function  $f_{bath}$  [34]

$$\begin{cases} \frac{d^2\bar{x}}{d\bar{t}^2} + (\bar{x} - \bar{v}\bar{t}) + \frac{u_0\pi\ell}{a} \sin \left( \frac{2\pi\ell}{a} \bar{x} \right) = f_{bath}(\bar{x}, \bar{t}), \\ \frac{d^2x_i}{d\bar{t}^2} + \omega_i^2 x_i = \frac{c_i}{m_i} \sin \left( \frac{2\pi\ell}{a} \bar{x} \right) \end{cases}, \tag{15}$$

$$f_{bath}(\bar{x}, \bar{t}) = \frac{2\pi\ell}{a} \left( \sum_i x_i c_i \right) \cos \left( \frac{2\pi\ell}{a} \bar{x} \right) - \frac{2\pi\ell}{a} \left( \sum_i \frac{c_i^2}{2m_i\omega_i^2} \right) \sin \left( \frac{4\pi\ell}{a} \bar{x} \right). \tag{16}$$



To solve the above system of equations, the bath degrees of freedom  $x_i$  are first resolved by using the Green function of the harmonic bath  $G(\bar{t}, \bar{t}') = \frac{1}{\omega_i} \Theta(\bar{t} - \bar{t}') \sin[\omega_i(\bar{t} - \bar{t}')] ]$  and taking into account the initial conditions  $x_i(0), v_i(0)$  of the external bath. This is followed by a summation of bath degrees of freedom using the spectral function  $J(\omega) = \sum_i \frac{c_i^2}{2m_i\omega_i} \delta(\omega - \omega_i) = 2\alpha\omega e^{-|\omega|/\omega_c}$  and the classical damping correlation  $\lim_{\omega_c \rightarrow \infty} \frac{4\alpha\omega_c}{1+\omega_c^2\bar{t}^2} = 4\pi\alpha\delta(\bar{t})$  following standard procedure [34]. Similar to the Caldeira-Leggett model discussed earlier,  $\alpha$  denotes the coupling parameter with the external bath and  $\omega_c$  is a cutoff frequency.

The bath coupling function can now be conveniently written as  $f_{bath}[\bar{x}(\bar{t}), \bar{t}] = f_{vis}[\bar{x}, \frac{d\bar{x}}{d\bar{t}}] + f_{ran}(\bar{t})$ , where

$$f_{vis}[\bar{x}, \frac{d\bar{x}}{d\bar{t}}] = -\frac{8\alpha\pi^3\ell^2}{a^2} \cos^2\left(\frac{2\pi\ell}{a}\bar{x}\right) \frac{d\bar{x}}{d\bar{t}}, \quad (17)$$

$$f_{ran}(\bar{t}) = \frac{2\pi\ell}{a} \left\{ \sum_i c_i \left[ x_i^{homo}(\bar{t}) - \sum_i \frac{c_i}{m_i\omega_i^2} \sin\left[\frac{2\pi\ell}{a}\bar{x}(0)\right] \cos(\omega_i\bar{t}) \right] \right\} \cos\left[\frac{2\pi\ell}{a}\bar{x}(\bar{t})\right]. \quad (18)$$

Since  $f_{vis}$  depends on position and velocity of the particle, but not on the initial conditions, this term is interpreted as an environmental viscous force [34]. The  $f_{ran}$  contribution depends on the initial conditions of the bath degrees of freedom and denotes the random force due to dissipation from the coupling to the external bath. At thermal equilibrium, the bath follows the canonical Maxwell-Boltzmann distribution, and as a result  $f_{ran}$  obeys the fluctuation-dissipation theorem [42] such that  $\langle f_{ran}(\bar{t})f_{ran}(\bar{t}') \rangle = k_B T \frac{8\alpha\pi^3\ell^2}{a^3} \cos^2\left[\frac{2\pi\ell}{a}\bar{x}(\bar{t})\right] \delta(\bar{t} - \bar{t}')$ . Details for the classical Prandtl-Tomlinson model in the presence of an external bath are given in section S-VI in the Supplementary Information [21].

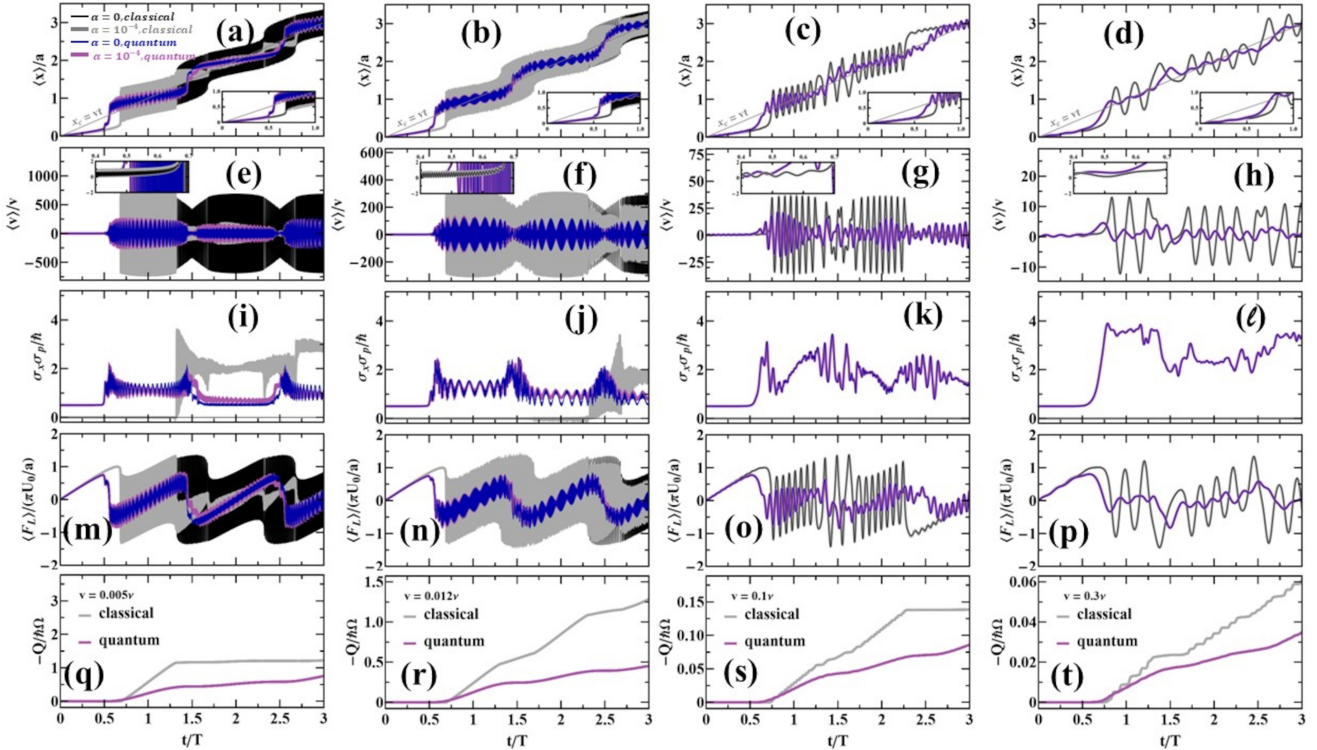


FIG. 3. Kinematic properties of the moving particle as function of  $t/T$ . The average displacement  $\langle x \rangle$  normalized by  $a$  for (a)  $v = 0.005\nu$ ; (b)  $v = 0.012\nu$ ; (c)  $v = 0.1\nu$ ; (d)  $v = 0.3\nu$ . The average velocity  $\langle v \rangle$  normalized by driving velocity of the harmonic trap  $v$  for (e)  $v = 0.005\nu$ ; (f)  $v = 0.012\nu$ ; (g)  $v = 0.1\nu$ ; (h)  $v = 0.3\nu$ . Standard deviation product  $\sigma_x \sigma_v / \hbar$  for (i)  $v = 0.005\nu$ ; (j)  $v = 0.012\nu$ ; (k)  $v = 0.1\nu$ ; (l)  $v = 0.3\nu$ . Lateral force  $\langle F_L \rangle$  normalized by  $\pi U_0/a$  (m)  $v = 0.005\nu$ ; (n)  $v = 0.012\nu$ ; (o)  $v = 0.1\nu$ ; (p)  $v = 0.3\nu$ . Dissipated heat  $-Q$  normalized by  $\hbar\Omega$  for (q)  $v = 0.005\nu$ ; (r)  $v = 0.012\nu$ ; (s)  $v = 0.1\nu$ ; (t)  $v = 0.3\nu$ .

### III. KINEMATIC AND DISSIPATIVE PROPERTIES OF THE MOVING NANOPARTICLE

The dissipative evolution of the particle/atomic chain system is further studied by examining its kinematic properties, as given in Table I. The moving particle is characterized by its instantaneous average position  $\langle x \rangle(\bar{t})$  and instantaneous average velocity  $\langle v \rangle(\bar{t})$ . Both are calculated for the closed particle/chain system governed by Eq. (1) and the particle/chain system with the external bath governed by Eq. (9). The results for  $\langle x \rangle(\bar{t})$  are given in Fig. 3 (a-d). Since the particle is guided forward by the optical trap, its instantaneous position  $x_c = vt$  is also shown. The results for  $\langle v \rangle(\bar{t})$  are given in Fig. 3 (e-h). In order to understand the quantum nature of the motion, the classical position  $x_{cl}$  and velocity  $v_{cl}$  calculated from the stochastic Newton second law of motion, as previously discussed, are also calculated and shown in Fig. 3.

By comparing the different regimes in Fig. 3(a-d), an emerging common feature is the smooth path in the first half of the period. Analyzing the states of the quantum system shows that in this region the particle remains localized in the minimum of the first well of the overall potential surface regardless of the driving velocity. At  $t/T \sim 0.5$  the particle becomes un-stuck and it slips into the second well of the potential surface (see section S-VIII in the Supplementary Information [21] for graphical details). In the case of a very slow driving velocity, the particle experiences almost frictionless motion in its initial stick-slip path since it remains in its ground state, as also seen in Fig. 2(e,i).

For driving velocities larger than the first Landau-Zener velocity  $v \gg v_{01}$ , the diabatic tunneling  $n = 0 \rightarrow n = 1$  at  $t/T \sim 0.5$  makes the state of the particle mainly distribute to the first excited state whose center moves from the second well back to the first well of the potential surface at  $t/T = 0.5$ . This diabatic Landau-Zener tunneling lengthens the stick-like motion path of the particle, contributing to an increased friction.

After the initial stick-slip motion, the particle is in a superposition state and it experiences a series of stick-slip oscillations with a frequency in the order of  $\Omega$ . Higher driving velocities involve contributions from higher states, which makes the stick-slip oscillations have more complex oscillatory patterns. Since the period of motion  $T$  is shortened for higher  $v$ , the number of oscillations in one period is reduced.

While the  $\langle x \rangle$  and  $\langle v \rangle$  for the closed and open quantum systems are very similar, there are differences when compared with the classical path. Fig. 3(a-d) shows that the classical particle also experiences stick-like motion, but at different times. For example, for  $v = 0.005v_0$ , the quantum slip occurs at  $t_{slip} \approx 0.49T$  while the classical slip occurs at  $t_{slip} \approx 0.65T$ . This trend also holds for higher driving velocities. A notable difference with the quantum mechanical motion is that the classical particle has to wait until the minimum of the first well of the potential surface completely disappears, which always happens later than  $t/T = 0.5$ . Since the stick path of the classical motion is much longer than the quantum one, the classical slip starts with higher energy leading to classical stick-slip oscillations with larger amplitudes. This delayed initial stick-slip and larger amplitude oscillations result in an enhanced classical friction compared to the quantum mechanical motion.

Fig. 3(a-h) further shows that the role of the heat bath is mostly pronounced for smaller driving velocities. Since  $T \sim 1/v$ , a smaller driving velocity leads to a longer period, hence environmental effects on the particle are better visible.

The instantaneous average velocity of the particle shown in Fig. 3(e-h) shows consistent with the displacement behavior. We find that during its initial  $t/T < 0.5$  time  $\langle v \rangle \approx 0$ . At the slipping moment at  $t/T \sim 0.5$ , the particle rapidly accelerates catching up with the driving trap. This is followed by oscillatory behavior in  $\langle v \rangle$  consistent with the oscillations in  $\langle x \rangle$ . Compared to the classical motion, however, the quantum  $\langle v \rangle$  oscillation always have smaller amplitudes since tunneling effects enhance the slipping forward of the particle.

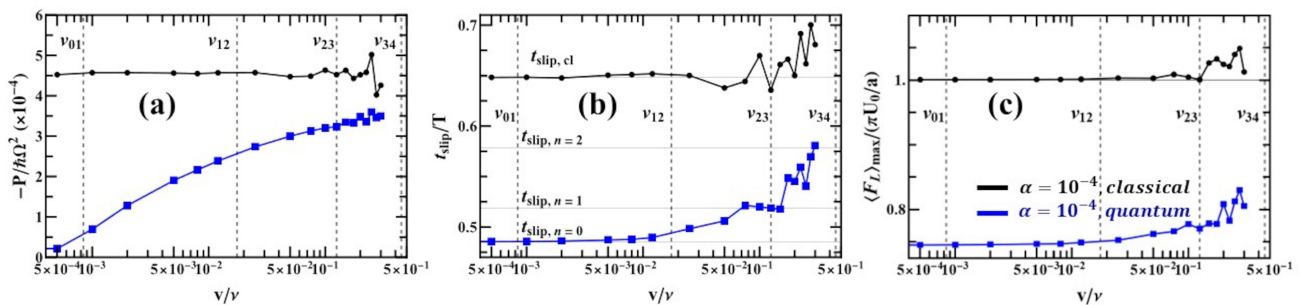


FIG. 4. Dynamic properties as a function of  $v/v_0$  calculated in the first period of the motion. (a) Released to the external bath power  $-P$  normalized by  $\hbar\Omega^2$ ; (b) The slipping time  $t_{slip}/T$  for a maximal lateral force; (c) The maximal lateral force  $\langle F_L \rangle_{max}$ . Classical (in black) and quantum mechanical (in blue) results are given. The diabatic tunneling velocities  $v_{ij}$  between the different instantaneous eigenstates are also shown.

Further insight into the  $\langle x \rangle$  and  $\langle v \rangle$  evolution can be gained by examining the time-dependence of their uncertainty principle. We find that  $\sigma_x \sigma_p = \hbar/2$  during the particle sticking period  $t/T < 0.5$  since the particle is confined in the ground state in the first well of the potential surface. For all later times  $\sigma_x \sigma_v > \hbar/2$  and it also shows oscillatory-like behavior. For the closed classical system  $\sigma_x \sigma_v = 0$  as expected, while for the open classical system  $\sigma_x \sigma_v > 0$  at around  $t/T \approx \frac{a^2}{(2\pi)^3 \hbar \alpha}$ .

We are now in a position to examine the evolution of the lateral force of the nanoparticle, typically measured via atomic force microscopy [43] or optical means [30, 31, 44]. The computed lateral force  $\langle F_L \rangle$  is defined as the spring force that holds the nanoparticle in the harmonic potential corrected by the motion of the optical trap, see I. The lateral force is a measure of the frictional force as the optical trap drags the particle above the atomic chain. The results shown in Fig.3(m,n,o,p) help us delineate quantum mechanical vs classical effects for different driving velocities. As the particle starts slipping at  $t/T \sim 0.5$  it catches up with the velocity of the driving trap and  $\langle F_L \rangle$  reaches its maximum. For small velocity, as mentioned above, the classical slipping occurs at the moment when the minimum of the first well of the potential surface diminishes, which happens at  $t_{slip}/T \approx \frac{1}{4} + \frac{\eta}{2\pi} \approx 0.65$ . The maximum classical lateral force is  $\langle F_L \rangle_{max} = \frac{\pi U_0}{a}$ . The quantum motion, on the other hand, pushes the slipping forward by 25% at  $t_{slip}/T \approx 0.49$  and the maximum quantum lateral force is smaller than classical one by 25% i.e.  $\langle F_L \rangle_{max} \approx 0.75 \left( \frac{\pi U_0}{a} \right)$ . For larger driving velocities, the quantum slipping happens at a later time, thus the maximum lateral force is larger than the one for smaller velocities.

In addition to the lateral force, the energy transfer between the moving particle and the external bath is also related to the frictional process. The transferred energy is expressed in terms of released to the environment heat ( $-Q$ ) defined as the difference between the energy of the particle and the work done by the moving trap (see Table I). Fig. 3(q-t) shows that during the stick-phase the nanoparticle does not exchange heat with the environment meaning that this regime is essentially friction-free. As the particle continues into its slip phase, higher energy levels are occupied. This excess above the ground state energy is being released to the environment marking the onset of dissipation. Comparing to the classical slipping, the quantum slipping generally occurs earlier, and as a result there is less dissipation since the quantum released heat is smaller than the classical one.

Let us now examine the velocity functional dependence of the dissipative motion of the nanoparticle. For this purpose, we track the power  $P$  associated with the released to the environment heat at the end of the first period and the maximum lateral force  $\langle F_L \rangle_{max}$  within that time frame. The results shown in Fig. 4(a,c) are presented together with the time  $t_{slip}$  in Fig. 4b characterizing the moment at which the lateral force becomes maximum in the first period of the motion for each velocity. Since the maximum lateral force signals the stick-slip transition, the times  $t_{slip,n}$  at which the different quantum eigenstates participate in this process are also shown in Fig. 4b. While the quantum particle dynamics is determined by a linear combination of the different eigenstates admixtures due to occurring Landau-Zener tunnelings, the classical particle with relatively slow velocity always stays at the minimum of the first potential [29, 45] well until  $t_{slip,cl}/T \approx \frac{1}{4} + \frac{\eta}{2\pi} \approx 0.647$ . For higher velocities, higher states of the Hamiltonian become important and in both, quantum and classical limits, the maximal lateral force, released heat, and slipping time can experience oscillatory-like features, as shown in Fig. 4.

The heat power in Fig. 4a shows a notable difference between the classical and quantum motion. Since the classical particle is stuck in the first minimum of the potential, the classical  $P$  is practically a constant over a large velocity range. For the quantum mechanical case, increasing the velocity causes an admixture of higher level eigenstates which results in an increasing released heat rate. Nevertheless, the quantum thermal power reaches about 75% of the classical value at  $v \geq v_{23}$ . A similar difference in magnitude is also found when comparing the classical and quantum maximum lateral force, as shown in Fig. 4c. We find that the classical  $\langle F_L \rangle_{max} \approx \frac{\pi U_0}{a}$  and it remains a constant over a large velocity range. The quantum  $\langle F_L \rangle_{max}$  is also a constant (75% of the classical one) although in a somewhat smaller velocity range.

#### IV. CONCLUSIONS

Friction at the nanoscale is a complex process, and here we offer a comprehensive study delineating quantum mechanical vs classical effects in the Prandtl-Tomlinson model, one of the most popular models in tribology. By focusing on the stick-slip regime (also captured in the classical corrugation parameter), it is found that Landau-Zener tunneling at multiple eigenenergy level anti-crossings is a quantum mechanical distinguishing factor. It is responsible for allowing the particle to permeate through the potential barriers, which are essentially impenetrable for the classical particle. As a result, the stick-slip quantum mechanical motion experiences reduced friction as compared to the classical case. The quantum mechanical effects in the nanoscaled friction are expected to play a reduced role at higher temperatures. As  $T$  is increased, higher states will become important leading to more pronounced classical

features in the motion of the particle.

The theoretical understanding is made possible by presenting the full description of the quantum mechanical and classical methodologies of Prandtl-Tomlinson model by distinguishing quantum vs classical vs dissipative aspects of the nanoscaled friction. A variety of properties are defined and examined in order to track the time dynamics and velocity functionality of the frictional process. Dissipative heat, dissipative thermal power, and lateral force can serve as a theoretical base for possible experimental probing of quantum effects in stick-slip motion. Moving cold atoms and ions in optical lattices and time-resolved Landau-Zener tunneling in periodic potentials, already achieved in the laboratory [30, 31, 46, 47], may be a useful platform to demonstrate the reduction of friction in the quantum mechanical regime.

## V. ACKNOWLEDGMENTS

L.M.W. acknowledges financial support from the US National Science Foundation under grant No. 2306203. P. R.-L. acknowledges support from Ministerio de Ciencia e Innovación (Spain), Agencia Estatal de Investigación, under project NAUTILUS (PID2022-139524NB-I00).




- 
- [1] A. I. Volokitin and B. N. J. Persson, Near-field radiative heat transfer and noncontact friction, *Rev. Mod. Phys.* **79**, 1291 (2007).
- [2] A. Vakis, V. Yastrebov, J. Scheibert, L. Nicola, D. Dini, C. Minfray, A. Almqvist, M. Paggi, S. Lee, G. Limbert, J. Molinari, G. Anciaux, R. Aghababaei, S. Echeverri Restrepo, A. Papangelo, A. Cammarata, P. Nicolini, C. Putignano, G. Carbone, S. Stupkiewicz, J. Lengiewicz, G. Costagliola, F. Bosia, R. Guarino, N. Pugno, M. Müser, and M. Ciavarella, Modeling and simulation in tribology across scales: An overview, *Tribol. Int.* **125**, 169 (2018).
- [3] M. Wolloch, G. Losi, M. Ferrario, and M. C. Righi, High-throughput screening of the static friction and ideal cleavage strength of solid interfaces, *Sci. Rep.* **9**, 17062 (2019).
- [4] S. Cahangirov, C. Ataca, M. Topsakal, H. Sahin, and S. Ciraci, Frictional Figures of Merit for Single Layered Nanostructures, *Phys. Rev. Lett.* **108**, 126103 (2012).
- [5] R. K. Barik and L. M. Woods, Frictional Properties of Two-Dimensional Materials: Data-Driven Machine Learning Predictive Modeling, *ACS Applied Materials & Interfaces* **16**, 40149 (2024), <https://doi.org/10.1021/acsami.4c05532>.
- [6] M. Wolloch, G. Levita, P. Restuccia, and M. C. Righi, Interfacial Charge Density and Its Connection to Adhesion and Frictional Forces, *Phys. Rev. Lett.* **121**, 026804 (2018).
- [7] P. C. Torche, A. Silva, D. Kramer, T. Polcar, and O. Hovorka, Multi-scale model predicting friction of crystalline materials, *Adv. Mater. Interfaces* **9**, 2100914 (2022).
- [8] I. Szlufarska, M. Chandross, and R. W. Carpick, Recent advances in single-asperity nanotribology, *J. Phys. D: Appl. Phys.* **41**, 123001 (2008).
- [9] G. Tomlinson, CVI. A molecular theory of friction, *London Edinb. Dublin Philos. Mag. J. Sci.* **7**, 905 (1929).
- [10] L. Prandtl, Ein Gedankenmodell zur kinetischen Theorie der festen Körper, *J. Appl. Math. Mech.* **8**, 85 (1928).
- [11] F. R. Krajewski and M. H. Müser, Quantum Creep and Quantum-Creep Transitions in 1D Sine-Gordon Chains, *Phys. Rev. Lett.* **92**, 030601 (2004).
- [12] F. R. Krajewski and M. H. Müser, Quantum dynamics in the highly discrete, commensurate Frenkel Kontorova model: A path-integral molecular dynamics study, *J. Chem. Phys.* **122**, 124711 (2005).
- [13] H. Xu, W. Chen, and Y. Zhu, Influence of the bond defect in driven Frenkel-Kontorova chains, *Phys. Rev. B* **75**, 224303 (2007).
- [14] L. Landau, Zur Theorie der Energieübertragung. II, *Physikalische Zeitschrift der Sowjetunion* **2**, 46–51 (1932).
- [15] C. Zener, Non-Adiabatic Crossing of Energy Levels, *Proc. R. Soc. London Ser. A* **137**, 696 (1932).
- [16] V. L. Pokrovsky and N. A. Sinitsyn, Landau-Zener transitions in a linear chain, *Phys. Rev. B* **65**, 153105 (2002).
- [17] Z. Huang and Y. Zhao, Dynamics of dissipative Landau-Zener transitions, *Phys. Rev. A* **97**, 013803 (2018).
- [18] T. Zanca, F. Pellegrini, G. E. Santoro, and E. Tosatti, Frictional lubricity enhanced by quantum mechanics, *Proc. Natl. Acad. Sci. U.S.A.* **115**, 3547 (2018).
- [19] L. Arceci, S. Barbarino, R. Fazio, and G. E. Santoro, Dissipative Landau-Zener problem and thermally assisted Quantum Annealing, *Phys. Rev. B* **96**, 054301 (2017).
- [20] A. Stone, *The Theory of Intermolecular Forces* (Oxford University Press, 2013).
- [21] See Supplementary Information for detail derivations of coupling potential between the nanoparticle and the atomic chain, matrix elements of quantum Prandtl-Tomlinson Hamiltonian in moving harmonic oscillator basis set, numerical calculation for quasi-static eigenenergies and eigenstates, quantum evolution with and without external bath reservoir, classical evolution with and without external bath reservoir; detail explanations for tunneling and slipping of quantum and classical trajectories and an animation (GIF) of quantum and classical motions; see also Refs. [48, 49] therein.
- [22] E. Meyer, T. Gyalog, R. M. Overney, and K. Dransfeld, *Nanoscience: Friction and Rheology on the Nanometer Scale* (World Scientific, 1998).



- [23] M. H. Müser, Velocity dependence of kinetic friction in the Prandtl-Tomlinson model, *Phys. Rev. B* **84**, 125419 (2011).
- [24] J. J. Sakurai and J. Napolitano, *Modern Quantum Mechanics*, 3rd ed. (Cambridge University Press, 2020).
- [25] M. Yamaguchi, T. Yuge, and T. Ogawa, Markovian quantum master equation beyond adiabatic regime, *Phys. Rev. E* **95**, 012136 (2017).
- [26] The considered time domain for the moving particle (from  $t_{min} = 0$  to  $t_{max} = 3T$  in this study) is divided evenly by infinitesimal small intervals  $\Delta t$  who must be smaller than the smallest period of Bohr oscillation between eigenstates  $\Delta t < |\max(E_n(\bar{t}) - E_m(\bar{t}))|^{-1}$ .
- [27] N. A. Peters, T.-C. Wei, and P. G. Kwiat, Mixed-state sensitivity of several quantum-information benchmarks, *Phys. Rev. A* **70**, 052309 (2004).
- [28] D. M. Tong, E. Sjöqvist, L. C. Kwek, and C. H. Oh, Kinematic Approach to the Mixed State Geometric Phase in Nonunitary Evolution, *Phys. Rev. Lett.* **93**, 080405 (2004).
- [29] A. Socoliuc, R. Bennewitz, E. Gnecco, and E. Meyer, Transition from Stick-Slip to Continuous Sliding in Atomic Friction: Entering a New Regime of Ultralow Friction, *Phys. Rev. Lett.* **92**, 134301 (2004).
- [30] D. Gangloff, A. Bylinskii, I. Counts, W. Jhe, and V. Vuletić, Velocity tuning of friction with two trapped atoms, *Nat. Phys.* **11**, 915–919 (2015).
- [31] I. Counts, D. Gangloff, A. Bylinskii, J. Hur, R. Islam, and V. Vuletić, Multislip Friction with a Single Ion, *Phys. Rev. Lett.* **119**, 043601 (2017).
- [32] D.-N. Le, N.-T. Hoang, and V.-H. Le, Exact analytical solutions of the schrödinger equation for a two dimensional purely sextic double-well potential, *Journal of Mathematical Physics* **59**, 032101 (2018), <https://doi.org/10.1063/1.4997532>.
- [33] A. O. Caldeira and A. J. Leggett, Influence of Dissipation on Quantum Tunneling in Macroscopic Systems, *Phys. Rev. Lett.* **46**, 211 (1981).
- [34] U. Weiss, *Quantum Dissipative Systems*, 4th ed. (World Scientific, Singapore, 2012).
- [35] T. Dittrich, P. Hänggi, G.-L. Ingold, B. Krammer, G. Schön, and W. Zwerger, *Quantum transport and dissipation* (Wiley-VCH, Weinheim, Germany, 1998).
- [36] S. Shevchenko, S. Ashhab, and F. Nori, Landau–zener–stüeckelberg interferometry, *Physics Reports* **492**, 1 (2010).
- [37] D. Bouwmeester, G. P. Karman, C. A. Schrama, and J. P. Woerdman, Observation of interference in transitions due to local geometric phases, *Phys. Rev. A* **53**, 985 (1996).
- [38] S. Gasparinetti, P. Solinas, and J. P. Pekola, Geometric landau-zener interferometry, *Phys. Rev. Lett.* **107**, 207002 (2011).
- [39] L. Viotti, F. C. Lombardo, and P. I. Villar, Geometric phase in a dissipative jaynes-cummings model: Theoretical explanation for resonance robustness, *Phys. Rev. A* **105**, 022218 (2022).
- [40] F. C. Lombardo and P. I. Villar, Geometric phases in open systems: A model to study how they are corrected by decoherence, *Phys. Rev. A* **74**, 042311 (2006).
- [41] L. Viotti, A. L. Gramajo, P. I. Villar, F. C. Lombardo, and R. Fazio, Geometric phases along quantum trajectories, *Quantum* **7**, 1029 (2023).
- [42] S. M. Rytov, Y. A. Kravtsov, and V. I. Tatarskii, *Principles of Statistical Radiophysics 3* (Springer, Berlin, Germany, 1989).
- [43] C.-W. Yang, K.-t. Leung, R.-F. Ding, H.-C. Ko, Y.-H. Lu, C.-K. Fang, and I.-S. Hwang, Lateral force microscopy of interfacial nanobubbles: Friction reduction and novel frictional behavior, *Scientific Reports* **8**, 3125 (2018).
- [44] E. Schäffer, S. F. Nørrelykke, and J. Howard, Surface forces and drag coefficients of microspheres near a plane surface measured with optical tweezers, *Langmuir* **23**, 3654 (2007).
- [45] E. Gnecco, R. Roth, and A. Baratoff, Analytical expressions for the kinetic friction in the Prandtl-Tomlinson model, *Phys. Rev. B* **86**, 035443 (2012).
- [46] E. Bonvin, L. Devaud, M. Rossi, A. Militaru, L. Dania, D. S. Bykov, M. Teller, T. E. Northup, L. Novotny, and M. Frimmer, Hybrid paul-optical trap with large optical access for levitated optomechanics, *Phys. Rev. Res.* **6**, 043129 (2024).
- [47] A. Zenesini, H. Lignier, G. Tayebirad, J. Radogostowicz, D. Ciampini, R. Mannella, S. Wimberger, O. Morsch, and E. Arimondo, Time-resolved measurement of landau-zener tunneling in periodic potentials, *Phys. Rev. Lett.* **103**, 090403 (2009).
- [48] I. S. Gradshteyn and I. M. Ryzhik, *Table of integrals, series, and products* (Academic press, 2014).
- [49] J. Wilkie and M. Çetinbaş, Variable-stepsize runge–kutta methods for stochastic schrödinger equations, *Physics Letters A* **337**, 166 (2005).



**Supplemental materials for:  
Quantum stick-slip motion in nanoscaled friction**

Dai-Nam Le <sup>1,\*</sup> , Pablo Rodriguez-Lopez <sup>2,†</sup> , Lilia M. Woods <sup>1,‡</sup> 

<sup>1</sup>*Department of Physics, University of South Florida, Tampa, Florida 33620, USA*

<sup>2</sup>*Área de Electromagnetismo and Grupo Interdisciplinar de Sistemas Complejos (GISC), Universidad Rey Juan Carlos, 28933, Móstoles, Madrid, Spain*

\* Email: [dainamle@usf.edu](mailto:dainamle@usf.edu); Homepage: <https://sites.google.com/view/dai-nam-le/>

† Email: [pablo.ropez@urjc.es](mailto:pablo.ropez@urjc.es)

‡ Corresponding author, Email: [lmwoods@usf.edu](mailto:lmwoods@usf.edu), Homepage: <https://www.amd-woods-group.com/>.

## CONTENTS

I. Introduction	1
II. Model System	2
A. Dynamics of the moving quantum particle: unitary evolution	3
B. Dynamics of the moving quantum particle with coupling to the environment	6
C. Dynamics of the moving particle within the classical Prandtl-Tomlinson model	7
III. Kinematic and Dissipative properties of the moving nanoparticle	9
IV. Conclusions	10
V. Acknowledgments	11
References	11
S-VI. Periodic potential from one-dimensional lattice	S-2
A. Short-range overlap interaction	S-2
B. Long-range vdW interaction	S-2
S-VII. Representation in moving harmonic oscillator basis set of wavefunctions	S-3
A. Basis set of moving harmonic oscillator	S-3
B. Matrix element of the periodic potential	S-3
S-VIII. Quasi-static eigenvalues and quasi-static eigenstates of our model	S-4
S-IX. Quantum dynamical evolution without environment	S-5
A. Explicit matrix elements $(\sigma_t)_{n,n'}(\bar{t})$ in the basis set of moving harmonic oscillator	S-6
B. Forth order Runge-Kutta solver for (S-23)	S-7
S-X. Quantum dynamical evolution with environment	S-7
1. Quantum theory of open system in weak coupling and Born-Markov approximations	S-7
2. Caldeira–Leggett model of thermal harmonic bath	S-10
3. Choice of $\mathcal{F}(\hat{x})$ and Matrix representations in the basis set of moving harmonic oscillator $ n^{(0)}(\bar{t})\rangle$	S-12
S-XI. Classical dynamical evolution with enviroment: the case of Caldeira-Leggett model	S-13
S-XII. Geometry phase	S-15
S-XIII. Tunneling and slipping of quantum quasi-static eigenstates and classical trajectory	S-16
S-XIV. Animation of quantum and classical motions	S-18
References	S-18

## S-VI. PERIODIC POTENTIAL FROM ONE-DIMENSIONAL LATTICE

### A. Short-range overlap interaction

Here we assume that the overlap interatomic interaction between the moving particle and a particle inside one-dimensional lattice exponentially decay since it is often that most of atoms' electron densities stay in their vdW radius and the overlap between electron densities is extremely small. Then the total short-range overlap interaction between the moving particle and one-dimensional chain is given as

$$V_{sr}(x) = - \sum_{n=-\infty}^{n=+\infty} A e^{-\frac{\sqrt{d^2+(x-na)^2}}{d_c}} \approx A e^{-\frac{d}{d_c}} \sum_{n=-\infty}^{n=+\infty} e^{-\frac{a^2}{2dd_c} \left(\frac{x}{a}-n\right)^2} = A e^{-\frac{d}{d_c}} \sqrt{\frac{2\pi dd_c}{a^2}} \vartheta_3 \left( \frac{\pi x}{a}, e^{-\frac{2\pi^2 dd_c}{a^2}} \right), \quad (\text{S-1})$$

where  $\vartheta_3(u, q) = 1 + 2 \sum_{n=1}^{+\infty} q^{n^2} \cos(2nu)$  is the third theta function. Here we consider the scenario when  $d \gg a$ ; thus, above potential becomes cosine one

$$V_{sr}(x) \approx A \sqrt{\frac{2\pi dd_c}{a^2}} e^{-\frac{d}{d_c}} \left[ 1 + 2e^{-\frac{2\pi^2 dd_c}{a^2}} \cos \left( \frac{2\pi x}{a} \right) \right]. \quad (\text{S-2})$$

### B. Long-range vdW interaction

For simplicity, we consider only  $C_6$  vdW interaction between the moving particle and a particle inside one-dimensional lattice; thus, the total long-range vdW interaction between the moving particle and one-dimensional chain is given as

$$\begin{aligned} V_{lr}(x) &= - \sum_{n=-\infty}^{n=+\infty} \frac{C_6}{[d^2 + (x-na)^2]^3} = \frac{C_6}{d^6} \sum_{n=-\infty}^{n=+\infty} \frac{1}{\left[ 1 + \frac{a^2}{d^2} \left( \frac{x}{a} - n \right)^2 \right]^3} \\ &= -\frac{C_6}{d^6} \times \left\{ \frac{3\pi d}{8a} \frac{\sinh\left(\frac{2\pi d}{a}\right)}{\cosh\left(\frac{2\pi d}{a}\right) - \cos\left(\frac{2\pi x}{a}\right)} + \frac{3\pi^2 d^2}{4a^2} \frac{\cosh\left(\frac{2\pi d}{a}\right) \cos\left(\frac{2\pi x}{a}\right) - 1}{[\cosh\left(\frac{2\pi d}{a}\right) - \cos\left(\frac{2\pi x}{a}\right)]^2} \right. \\ &\quad \left. + \frac{\pi^3 d^3}{2a^3} \frac{\sinh\left(\frac{2\pi d}{a}\right) [\cosh\left(\frac{2\pi d}{a}\right) \cos\left(\frac{2\pi x}{a}\right) + \cos^2\left(\frac{2\pi x}{a}\right) - 2]}{[\cosh\left(\frac{2\pi d}{a}\right) - \cos\left(\frac{2\pi x}{a}\right)]^3} \right\}. \end{aligned} \quad (\text{S-3})$$

When the distance between the moving particle and one-dimensional chain is large  $d \gg a$ , the long-range vdW interaction approximately becomes a cosine potential

$$V_{lr}(x) \approx -\frac{3\pi C_6}{8d^5 a} \left[ 1 + 2e^{-\frac{2\pi d}{a}} \cos \left( \frac{2\pi x}{a} \right) \right]. \quad (\text{S-4})$$

Combining the repulsive short-range overlap and attractive long-range vdW interaction given in Equations (S-2) and (S-4), the interaction arising from one-dimensional chain of atoms is approximately given as

$$V(x) = V_{sr}(x) + V_{lr}(x) \approx \left[ A \sqrt{\frac{2\pi dd_c}{a^2}} e^{-\frac{d}{d_c}} - \frac{3\pi C_6}{8d^5 a} \right] + 2 \left[ A \sqrt{\frac{2\pi dd_c}{a^2}} e^{-\frac{d}{d_c} - \frac{2\pi^2 dd_c}{a^2}} - \frac{3\pi C_6}{8d^5 a} e^{-\frac{2\pi d}{a}} \right] \cos \left( \frac{2\pi x}{a} \right). \quad (\text{S-5})$$

Denote  $U_0(d) = 4 \left[ A \sqrt{\frac{2\pi dd_c}{a^2}} e^{-\frac{d}{d_c} - \frac{2\pi^2 dd_c}{a^2}} - \frac{3\pi C_6}{8d^5 a} e^{-\frac{2\pi d}{a}} \right]$  and  $\Delta_0(d) = \left[ A \sqrt{\frac{2\pi dd_c}{a^2}} e^{-\frac{d}{d_c}} - \frac{3\pi C_6}{8d^5 a} \right] - \frac{1}{2} U_0(d)$ , then the resulting potential by one-dimensional chain of atom can be represented in a more compact form

$$V(x) = \Delta_0(d) + \frac{U_0(d)}{2} + \frac{U_0(d)}{2} \cos \left( \frac{2\pi x}{a} \right) = \Delta_0(d) + U_0(d) \sin^2 \left( \frac{\pi x}{a} \right). \quad (\text{S-6})$$

## S-VII. REPRESENTATION IN MOVING HARMONIC OSCILLATOR BASIS SET OF WAVEFUNCTIONS

### A. Basis set of moving harmonic oscillator

To perform any calculations in this study, we need to choose a basis set of wavefunctions where any arbitrary state can be expressed as a superposition of these basis wavefunctions. In our model's Hamiltonian  $H_S(\bar{t})$ , the periodic potential has a finite height, while a moving harmonic trap potential has an infinite height. Thus two most natural choice of basis set are the eigenstates of the periodic potential and the eigenstates of the harmonic oscillator. Both choices have pros and cons. Indeed, since the periodic potential is time independent, its eigenstates are time independent and orthonormalized. However, the harmonic trap potential is more dominant when the particle is far from the center of the trap and consequently, the particle wavefunction will tend to localized inside the harmonic trap. This localization property cannot be satisfied by eigenstates of periodic potential because these eigenstates obey Bloch theorem. One will need to Wannierized these eigenstates in order to control the convergence of the calculations; for an example, see Ref. [18]. The eigenstates of the harmonic oscillator, on the other hand, will automatically obey the required localization property. But since the harmonic trap is moving, we need to pick the eigenstates of a moving harmonic oscillator (The upper index  $\dots^{(0)}$  stands for solutions without periodic potential i.e  $u_0 = 0$ ):

$$E_n^{(0)} = n + \frac{1}{2}, \quad |n^{(0)}(\bar{t})\rangle = \varphi_0^{HO}(\bar{x} - \bar{v}\bar{t}) = \frac{1}{\sqrt{2^n n! \sqrt{\pi}}} e^{-\frac{(\bar{x} - \bar{v}\bar{t})^2}{2}} H_n(\bar{x} - \bar{v}\bar{t}), \quad (\text{S-7})$$

where  $H_n$  is  $n$ -th Hermite polynomials [24]. Noticeably, this basis set of wavefunctions relates to the basis set of wavefunctions of the static harmonic oscillator  $|n^{(0)}(0)\rangle = \varphi_0^{HO}(\bar{x})$  by the following expansions

$$|n^{(0)}(\bar{t})\rangle = \sum_{p=0}^{+\infty} c_{np}^{(0)}(\bar{t}) |n^{(0)}(0)\rangle, \quad |n^{(0)}(0)\rangle = \sum_{p=0}^{+\infty} c_{pn}^{(0)*}(\bar{t}) |n^{(0)}(\bar{t})\rangle, \quad (\text{S-8})$$

where  $c_{np}^{(0)}(\bar{t}) = e^{-\frac{\bar{v}^2 \bar{t}^2}{4}} \sum_{m=0}^{\min(n,p)} \frac{(-1)^{n-m}}{m!(n-m)!(p-m)!} \sqrt{\frac{n!p!}{2^{n+p-2m}}} (\bar{v}\bar{t})^{n+p-2m}$ .

### B. Matrix element of the periodic potential

Next, we need to evaluate the matrix elements of the periodic potential in the representation of the moving harmonic oscillator basis set. To do so, there are two necessary integrals need to be given [48]

$$\begin{aligned} I_{pp'} &= \frac{1}{\sqrt{2^{p+p'} p! p'! \sqrt{\pi}}} \int_0^{+\infty} e^{-\bar{x}^2} \cos\left(\frac{2\pi\ell}{a}\bar{x}\right) H_p(\bar{x}) H_{p'}(\bar{x}) \\ &= \begin{cases} 0 & \text{when } |p-p'| \text{ is odd} \\ \frac{(-1)^{\frac{|p-p'|}{2}}}{\sqrt{2^{|p-p'|+2}}} \sqrt{\frac{\min(p,p')!}{\max(p,p')!}} \left(\frac{2\pi\ell}{a}\right)^{|p-p'|} e^{-\frac{1}{4}\left(\frac{2\pi\ell}{a}\right)^2} \mathcal{L}_{\min(p,p')}^{|p-p'|} \left[\frac{1}{2}\left(\frac{2\pi\ell}{a}\right)^2\right] & \text{when } |p-p'| \text{ is even} \end{cases} \end{aligned} \quad (\text{S-9})$$

and

$$\begin{aligned} J_{pp'} &= \frac{1}{\sqrt{2^{p+p'} p! p'! \sqrt{\pi}}} \int_0^{+\infty} e^{-\bar{x}^2} \sin\left(\frac{2\pi\ell}{a}\bar{x}\right) H_p(\bar{x}) H_{p'}(\bar{x}) \\ &= \begin{cases} \frac{(-1)^{\frac{|p-p'|-1}{2}}}{\sqrt{2^{|p-p'|-2}}} \sqrt{\frac{\min(p,p')!}{\max(p,p')!}} \left(\frac{2\pi\ell}{a}\right)^{|p-p'|} e^{-\frac{1}{4}\left(\frac{2\pi\ell}{a}\right)^2} \mathcal{L}_{\min(p,p')}^{|p-p'|} \left[\frac{1}{2}\left(\frac{2\pi\ell}{a}\right)^2\right] & \text{when } |p-p'| \text{ is odd} \\ 0 & \text{when } |p-p'| \text{ is even} \end{cases} \end{aligned} \quad (\text{S-10})$$

Now, rewriting the periodic potential as

$$\sin^2\left(\frac{\pi\ell}{a}\bar{x}\right) - \frac{1}{2} = -\frac{1}{2} u_0 \cos\left(\frac{2\pi\ell}{a}\bar{x}\right) = -\frac{1}{2} \left[ \cos\left(\frac{2\pi\ell}{a}\bar{v}\bar{t}\right) \cos\left(\frac{2\pi\ell}{a}(\bar{x} - \bar{v}\bar{t})\right) - \sin\left(\frac{2\pi\ell}{a}\bar{v}\bar{t}\right) \sin\left(\frac{2\pi\ell}{a}(\bar{x} - \bar{v}\bar{t})\right) \right], \quad (\text{S-11})$$

then using (S-7) to obtain matrix elements of  $\hat{V}_{cos}$ :

$$\mathcal{V}_{n,n'}(\bar{t}) = - \left[ \cos \left( \frac{2\pi\ell}{a} \bar{v}\bar{t} \right) I_{nn'} - \sin \left( \frac{2\pi\ell}{a} \bar{v}\bar{t} \right) J_{nn'} \right] = \begin{cases} + \sin \left( \frac{2\pi\ell}{a} \bar{v}\bar{t} \right) J_{nn'} & \text{when } |n - n'| \text{ is odd} \\ - \cos \left( \frac{2\pi\ell}{a} \bar{v}\bar{t} \right) I_{nn'} & \text{when } |n - n'| \text{ is even} \end{cases}, \quad (\text{S-12})$$

where  $I_{nn'}$  and  $J_{nn'}$  are explicitly given in Equations (S-9) and (S-10). Based on known matrix elements  $\mathcal{V}_{n,n'}(\bar{t})$ , the matrix representation of the original Hamiltonian is finally obtained

$$(H_S)_{n,n'}(\bar{t}) = \langle n^{(0)}(\bar{t}) | \hat{H}_S(t) | n'^{(0)}(\bar{t}) \rangle = \left( n + \frac{1}{2} + \frac{1}{2}u_0 \right) \delta_{n,n'} + u_0 \mathcal{V}_{n,n'}(\bar{t}). \quad (\text{S-13})$$

### S-VIII. QUASI-STATIC EIGENVALUES AND QUASI-STATIC EIGENSTATES OF OUR MODEL

Now we are looking for the solution of the quasi-static a.k.a time-independent Schrödinger equation where time  $t$  plays a role as a parameter

$$\hat{H}_S(t) |n(\bar{t})\rangle = E_n(t) |n(\bar{t})\rangle. \quad (\text{S-14})$$

Utilizing  $\varphi_n^{(0)}(\bar{x}, \bar{t})$  as basic set of wavefunctions, our eigenstates can be rewritten as

$$\langle \bar{x} | n(\bar{t}) \rangle = \psi_n(\bar{x}, \bar{t}) = \sum_{p'=0}^{\infty} c_{n,p'}(\bar{t}) \varphi_{p'}^{(0)}(\bar{x}, \bar{t}), \quad \sum_{p'=0}^{\infty} |c_{n,p'}(\bar{t})|^2 = 1. \quad (\text{S-15})$$

Substituting (S-15) into (S-14), then multiplying both sides with  $\varphi_p^{(0)}(\bar{x}, \bar{t})$  followed by integrating both sides with  $\bar{x}$  from  $-\infty$  to  $\infty$  and noticing the orthonormality of the basis set  $\varphi_n^{(0)}(\bar{x}, \bar{t})$ , we finally obtain the following eigenvalue equation

$$\sum_{p'=0}^{\infty} (H_S)_{p,p'}(\bar{t}) c_{n,p'}(\bar{t}) = E_n(\bar{t}) c_{n,p}(\bar{t}), \quad (\text{S-16})$$

where  $E_n(\bar{t})$  is eigenvalue of the matrix  $(H_S)_{n,n'}(\bar{t})$  while  $[c_{n,0}(\bar{t}), c_{n,1}(\bar{t}), c_{n,2}(\bar{t}), \dots]^T$  is the corresponding eigenvector.

Diagonalize the matrix  $(H_S)_{n,n'}(\bar{t})$ , we can find the eigenvalues of  $\hat{H}_S(\bar{t})$ . In reality, the diagonalization is applied for finite size  $N_{size}$  of matrix representation of  $\hat{H}_S(\bar{t})$  where  $N_{size}$  is sufficiently large enough. For example, Figure S-1 below illustrates the convergence test of the first five eigenvalues in the case of  $u_0 = 5$  and  $a = 2\pi\ell$  when  $N_{size}$  increases from 5 to 50. As our examination, if looking up to the first 5 eigenvalues,  $N_{size}$  should be larger than 15 to gain enough precision. In further examinations, we set  $N_{size} = 25$  in order to balance accuracy and efficiency.

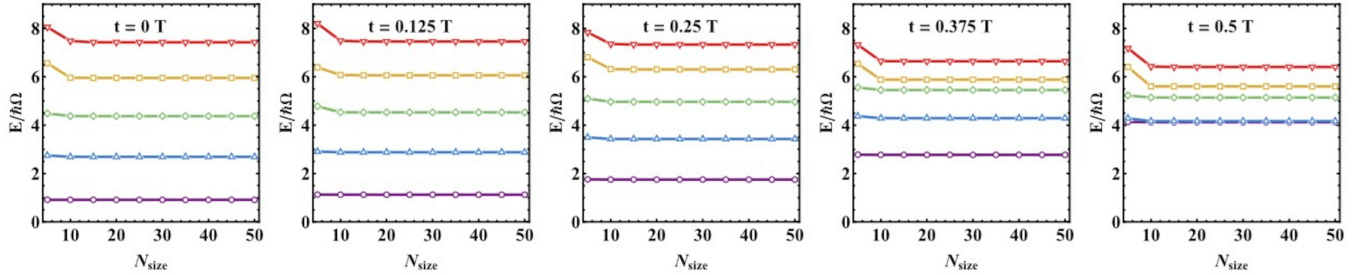


FIG. S-1. First 5 eigenvalues versus the finite size  $N_{size}$  when increasing  $N_{size}$  from 5 to 50 for different points of time.

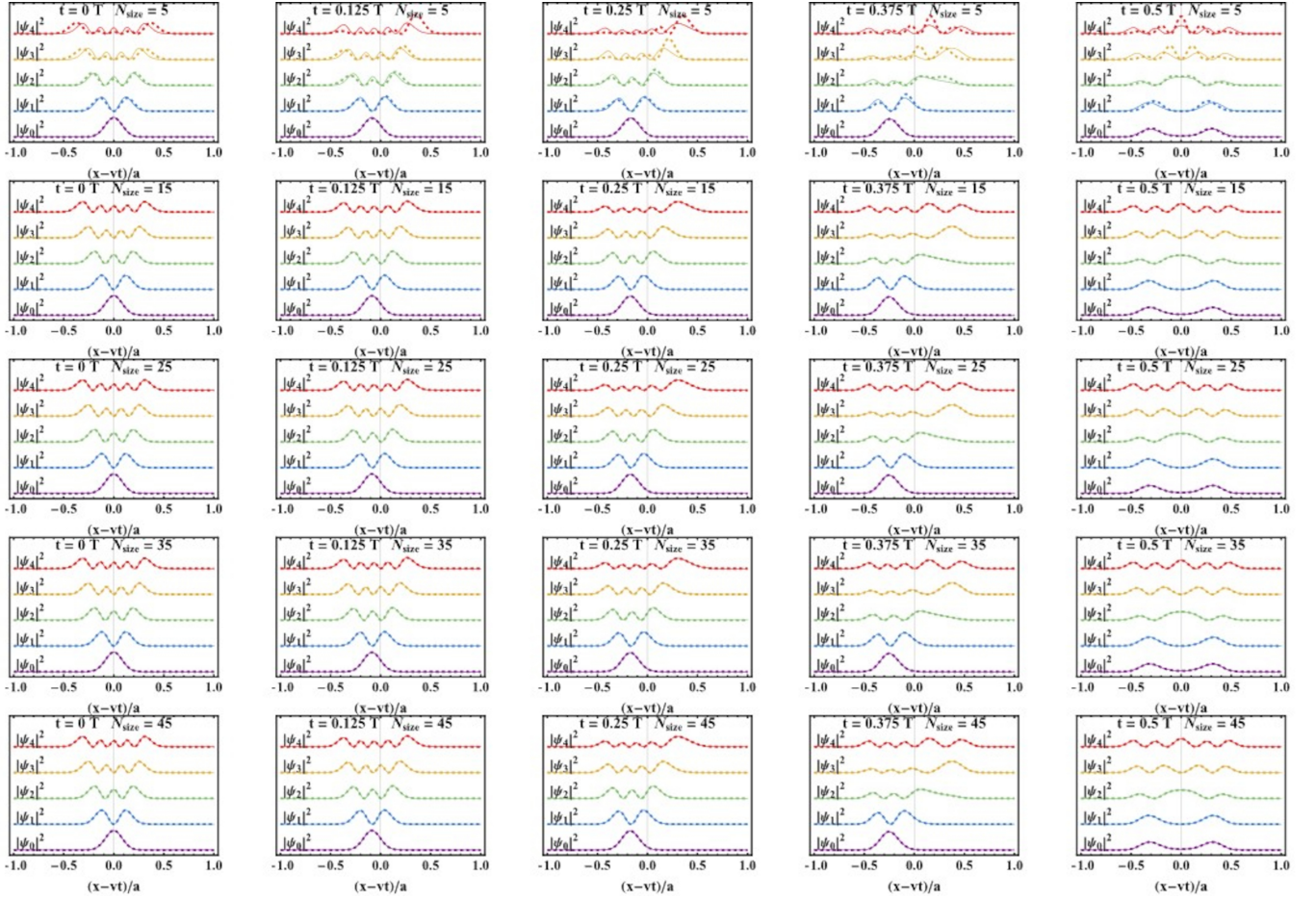


FIG. S-2. First 5 eigenstates versus the finite size  $N_{size}$  when increasing  $N_{size}$  from 5 to 45 for different points of time (dotted lines). As a benchmark, results with  $N_{size} = 50$  are also given (solid lines).

### S-IX. QUANTUM DYNAMICAL EVOLUTION WITHOUT ENVIRONMENT

Dynamical evolution of a closed system is governed by the following quantum Liouville–von Neumann equation

$$\frac{d}{dt}\hat{\rho}_S(t) = \frac{1}{i\hbar} \left[ \hat{H}_S(t), \hat{\rho}_S(t) \right], \quad (\text{S-17})$$

where density matrix operator  $\hat{\rho}_S(t)$  captures all dynamical information about our quantum system. Noticeably that we are working in dimensionless Hamiltonian by setting  $\hbar = 1$  and replacing  $t$  by  $\bar{t}$ ; therefore, dimensionless form of quantum Liouville–von Neumann equation is

$$\frac{d}{d\bar{t}}\hat{\rho}_S(\bar{t}) = -i \left[ \hat{H}_S(\bar{t}), \hat{\rho}_S(\bar{t}) \right], \quad (\text{S-18})$$

In the basis  $|n^{(0)}(\bar{t})\rangle$ , the matrix representation of density matrix operator  $\hat{\rho}_S(\bar{t})$  is given as

$$(\rho_S)_{n,n'}(\bar{t}) = \left\langle n^{(0)}(\bar{t}) \left| \hat{\rho}_S(\bar{t}) \right| n'^{(0)}(\bar{t}) \right\rangle, \quad (\text{S-19})$$

while the time derivative operator  $i \frac{d}{d\bar{t}}$  is represented by the following matrix

$$(\sigma_t)_{n,n'}(\bar{t}) = i \left\langle n^{(0)}(\bar{t}) \left| \left( \frac{d}{d\bar{t}} \right) \right| n'^{(0)}(\bar{t}) \right\rangle. \quad (\text{S-20})$$



We will determine the explicit expression of matrix  $(\sigma_t)_{n,n'}(\bar{t})$  later. According to the orthonormal of the chosen basis  $|n^{(0)}(\bar{t})\rangle$ , we can easily show that

$$\begin{aligned} \frac{d}{d\bar{t}} \langle n^{(0)}(\bar{t}) | n'^{(0)}(\bar{t}) \rangle = 0 &\Rightarrow \langle n^{(0)}(\bar{t}) | \left( \frac{d}{d\bar{t}} | n'^{(0)}(\bar{t}) \rangle \right) + \left( \frac{d}{d\bar{t}} \langle n^{(0)}(\bar{t}) | \right) | n'^{(0)}(\bar{t}) \rangle = 0 \\ &\Rightarrow i \left( \frac{d}{d\bar{t}} \langle n^{(0)}(\bar{t}) | \right) | n'^{(0)}(\bar{t}) \rangle = -(\sigma_t)_{n,n'}(\bar{t}). \end{aligned} \quad (\text{S-21})$$

From (S-18) we have

$$\begin{aligned} &\frac{d}{d\bar{t}} \left\{ \sum_{n,n'} (\rho_S)_{n,n'}(\bar{t}) | n^{(0)}(\bar{t}) \rangle \langle n'^{(0)}(\bar{t}) | \right\} = -i \sum_{n,n'} [H_S(\bar{t}), \rho_S(\bar{t})]_{n,n'} | n^{(0)}(\bar{t}) \rangle \langle n'^{(0)}(\bar{t}) | \\ \Leftrightarrow &\sum_{n,n'} \frac{d(\rho_S)_{n,n'}(\bar{t})}{d\bar{t}} | n^{(0)}(\bar{t}) \rangle \langle n'^{(0)}(\bar{t}) | + \sum_{n'',n'} (\rho_S)_{n'',n'}(\bar{t}) \left( \frac{d}{d\bar{t}} | n''^{(0)}(\bar{t}) \rangle \right) \langle n'^{(0)}(\bar{t}) | \\ &+ \sum_{n,n''} (\rho_S)_{n,n''}(\bar{t}) | n^{(0)}(\bar{t}) \rangle \left( \frac{d}{d\bar{t}} \langle n''^{(0)}(\bar{t}) | \right) = -i \sum_{n,n'} [H_S(\bar{t}), \rho_S(\bar{t})]_{n,n'} | n^{(0)}(\bar{t}) \rangle \langle n'^{(0)}(\bar{t}) | \\ \Leftrightarrow &\sum_{n,n'} \frac{d(\rho_S)_{n,n'}(\bar{t})}{d\bar{t}} | n^{(0)}(\bar{t}) \rangle \langle n'^{(0)}(\bar{t}) | + \sum_{n,n',n''} (\rho_S)_{n'',n'}(\bar{t}) \left[ | n^{(0)}(\bar{t}) \rangle \left( \frac{d}{d\bar{t}} | n''^{(0)}(\bar{t}) \rangle \right) \right] | n^{(0)}(\bar{t}) \rangle \langle n'^{(0)}(\bar{t}) | \\ &+ \sum_{n,n'} (\rho_S)_{n,n',n''}(\bar{t}) | n^{(0)}(\bar{t}) \rangle \left[ \left( \frac{d}{d\bar{t}} \langle n''^{(0)}(\bar{t}) | \right) | n'^{(0)}(\bar{t}) \rangle \right] \langle n'^{(0)}(\bar{t}) | = -i \sum_{n,n'} [H_S(\bar{t}), \rho_S(\bar{t})]_{n,n'} | n^{(0)}(\bar{t}) \rangle \langle n'^{(0)}(\bar{t}) | \\ \Leftrightarrow &\sum_{n,n'} \frac{d(\rho_S)_{n,n'}(\bar{t})}{d\bar{t}} | n^{(0)}(\bar{t}) \rangle \langle n'^{(0)}(\bar{t}) | - i \sum_{n,n',n''} (\sigma_t)_{n,n''}(\bar{t}) (\rho_S)_{n'',n'}(\bar{t}) | n^{(0)}(\bar{t}) \rangle \langle n'^{(0)}(\bar{t}) | \\ &+ i \sum_{n,n'} (\rho_S)_{n,n',n''}(\bar{t}) (\sigma_t)_{n'',n'}(\bar{t}) | n^{(0)}(\bar{t}) \rangle \langle n'^{(0)}(\bar{t}) | = -i \sum_{n,n'} [H_S(\bar{t}), \rho_S(\bar{t})]_{n,n'} | n^{(0)}(\bar{t}) \rangle \langle n'^{(0)}(\bar{t}) | \\ \Leftrightarrow &\sum_{n,n'} \frac{d(\rho_S)_{n,n'}(\bar{t})}{d\bar{t}} | n^{(0)}(\bar{t}) \rangle \langle n'^{(0)}(\bar{t}) | - i \sum_{n,n'} [\sigma_t(\bar{t}), \rho_S(\bar{t})]_{n,n'} | n^{(0)}(\bar{t}) \rangle \langle n'^{(0)}(\bar{t}) | \\ &= -i \sum_{n,n'} [H_S(\bar{t}), \rho_S(\bar{t})]_{n,n'} | n^{(0)}(\bar{t}) \rangle \langle n'^{(0)}(\bar{t}) | \\ \Leftrightarrow &\sum_{n,n'} \frac{d(\rho_S)_{n,n'}(\bar{t})}{d\bar{t}} | n^{(0)}(\bar{t}) \rangle \langle n'^{(0)}(\bar{t}) | = -i \sum_{n,n'} [H_S(\bar{t}) - \sigma_t(\bar{t}), \rho_S(\bar{t})]_{n,n'} | n^{(0)}(\bar{t}) \rangle \langle n'^{(0)}(\bar{t}) |. \end{aligned} \quad (\text{S-22})$$

or as the first-order ordinary differential equation of matrix:

$$\frac{d}{d\bar{t}} \rho_S(\bar{t}) = -i [H_S(\bar{t}) - \sigma_t(\bar{t}), \rho_S(\bar{t})]. \quad (\text{S-23})$$

### A. Explicit matrix elements $(\sigma_t)_{n,n'}(\bar{t})$ in the basis set of moving harmonic oscillator

First of all, we have to notice that if denote  $\bar{x}' = \bar{x} - \bar{v}\bar{t}$  then

$$i \frac{d}{d\bar{t}} | n^{(0)}(\bar{t}) \rangle = i \frac{d}{d\bar{t}} \varphi_n^{HO}(\bar{x} - \bar{v}\bar{t}) = \bar{v} \left( -i \frac{d}{d\bar{x}'} \varphi_n^{HO}(\bar{x}') \right) = \bar{v} \left( \hat{p}' \varphi_n^{HO}(\bar{x}') \right). \quad (\text{S-24})$$

The action of momentum operator on an eigenstate of a harmonic oscillator can be found in any quantum mechanics textbook [24]

$$\hat{p}' \varphi_n^{HO}(\bar{x}') = \frac{i}{\sqrt{2}} [\sqrt{n+1} \varphi_{n+1}^{HO}(\bar{x}') - \sqrt{n} \varphi_{n-1}^{HO}(\bar{x}')] = \frac{i}{\sqrt{2}} [\sqrt{n+1} \varphi_{n+1}^{(0)}(\bar{x}, \bar{t}) - \sqrt{n} \varphi_{n-1}^{(0)}(\bar{x}, \bar{t})], \quad (\text{S-25})$$

thus, Equation (S-24) becomes

$$i \frac{d}{dt} \varphi_n^{(0)}(\bar{x}, \bar{t}) = \frac{i \bar{v}}{\sqrt{2}} \left[ \sqrt{n+1} \varphi_{n+1}^{(0)}(\bar{x}, \bar{t}) - \sqrt{n} \varphi_{n-1}^{(0)}(\bar{x}, \bar{t}) \right], \quad (\text{S-26})$$

or

$$i \frac{d}{dt} |n^{(0)}(\bar{t})\rangle = \frac{i \bar{v}}{\sqrt{2}} \left[ \sqrt{n+1} |(n+1)^{(0)}(\bar{t})\rangle - \sqrt{n} |(n-1)^{(0)}(\bar{t})\rangle \right]. \quad (\text{S-27})$$

Plugging (S-27) in (S-20), we finally find matrix elements  $(\sigma_t)_{n,n'}(\bar{t})$  explicitly as

$$(\sigma_t)_{n,n'}(\bar{t}) = \frac{i \bar{v}}{\sqrt{2}} \left( \sqrt{n'+1} \delta_{n,n'+1} - \sqrt{n'} \delta_{n,n'-1} \right) = \frac{i \bar{v}}{\sqrt{2}} \left( \sqrt{n'+1} \delta_{n,n'+1} - \sqrt{n+1} \delta_{n+1,n'} \right) \equiv (\sigma_t)_{n,n'}. \quad (\text{S-28})$$

Hence  $\sigma_t(\bar{t})$  is a time-independent Hermitian tridiagonal matrix with zero main diagonal

$$\sigma_t = \sigma_t^\dagger = \frac{\bar{v}}{\sqrt{2}} \begin{pmatrix} 0 & -i\sqrt{1} & 0 & 0 & 0 & \dots \\ i\sqrt{1} & 0 & -i\sqrt{2} & 0 & 0 & \dots \\ 0 & i\sqrt{2} & 0 & -i\sqrt{3} & 0 & \dots \\ 0 & 0 & i\sqrt{3} & 0 & -i\sqrt{4} & \dots \\ 0 & 0 & 0 & i\sqrt{4} & 0 & \dots \\ \vdots & \vdots & \vdots & \vdots & \vdots & \ddots \end{pmatrix} \quad (\text{S-29})$$

### B. Forth order Runge-Kutta solver for (S-23)

To solve the first-order ordinary differential equation of matrix (S-23), we utilize a forth order Runge-Kutta method (RK4) by dividing time domain from  $\bar{t} = 0$  to  $\bar{t} = \bar{t}_{max}$  by even grid spacing by  $\Delta\bar{t}$ . Then density matrix at  $\bar{t} + \Delta\bar{t}$  is obtained by

$$\rho_S(\bar{t} + \Delta\bar{t}) = \rho_S(\bar{t}) + \frac{1}{6} (\kappa_1 + 2\kappa_2 + 2\kappa_3 + \kappa_4) \Delta\bar{t}, \quad (\text{S-30})$$

$$\begin{cases} \kappa_1 = -i [H_S(\bar{t}) - \sigma_t(\bar{t}), \rho_S(\bar{t})] \\ \kappa_2 = -i [H_S(\bar{t} + \frac{1}{2}\Delta\bar{t}) - \sigma_t(\bar{t} + \frac{1}{2}\Delta\bar{t}), \rho_S(\bar{t}) + \frac{1}{2}\kappa_1\Delta\bar{t}] \\ \kappa_3 = -i [H_S(\bar{t} + \frac{1}{2}\Delta\bar{t}) - \sigma_t(\bar{t} + \frac{1}{2}\Delta\bar{t}), \rho_S(\bar{t}) + \frac{1}{2}\kappa_2\Delta\bar{t}] \\ \kappa_4 = -i [H_S(\bar{t} + \Delta\bar{t}) - \sigma_t(\bar{t} + \Delta\bar{t}), \rho_S(\bar{t}) + \kappa_3\Delta\bar{t}] \end{cases}.$$

From a given initial density matrix  $\rho_S(0)$ , (S-30) can help us determine the dynamical evolution of  $\hat{\rho}_S(t)$ . However, the big issue of forth-order Runge-Kutta method is the positiveness of density matrix. This method is shown not to preserve the positiveness of the density matrix. Therefore, we may need a better solver for equation (S-23).

## S-X. QUANTUM DYNAMICAL EVOLUTION WITH ENVIRONMENT

### 1. Quantum theory of open system in weak coupling and Born-Markov approximations

Let us consider the general Hamiltonian describing a system ( $S$ ) interacting with a surrounding environment i.e bath ( $B$ ) [25]

$$\hat{H}(t) = \hat{H}_S(t) \otimes \hat{1}_B + \hat{1}_S \otimes \hat{H}_B + \lambda \hat{H}_{SB}(t), \quad (\text{S-31})$$

where the interacting Hamiltonian  $\hat{H}_{SB}(t)$  generally takes the following form

$$\hat{H}_{SB}(t) = \sum_{\alpha} A_{\alpha}(t) \otimes B_{\alpha} = \sum_{\alpha} A_{\alpha}^{\dagger}(t) \otimes B_{\alpha}^{\dagger}. \quad (\text{S-32})$$

In (S-31), dimensionless factor  $\lambda$  is introduced to manipulate the magnitude of the interaction from non-interacting case  $\lambda = 0$  to the full interacting case  $\lambda = 1$ . In the final result, we will put  $\lambda = 1$ .

In Schrödinger picture, the quantum Liouville–von Neumann equation of the whole system ( $S + B$ ) is

$$\frac{d}{dt}\hat{\rho}(t) = \frac{1}{i\hbar} [\hat{H}, \hat{\rho}]. \quad (\text{S-33})$$

Instead of Schrödinger picture, we can move to the interaction picture where an operator  $\hat{O}(t)$  is replaced by

$$\check{O}(t) = \hat{U}_{S+B}(t, t_0) \hat{O}(t) \hat{U}_{S+B}^\dagger(t, t_0), \quad (\text{S-34})$$

where  $U_{S+B}(t, t_0)$  is time evolution operator of non-interacting system  $(S + B)_{\lambda=0}$

$$\hat{U}_{S+B}(t, t') = \begin{cases} \mathcal{T}_+ \exp\left(-\frac{i}{\hbar} \int_{t'}^t \hat{H}_S(s) ds\right) & t > t' \\ \mathcal{T}_- \exp\left(+\frac{i}{\hbar} \int_t^{t'} \hat{H}_S(s) ds\right) & t < t' \end{cases} \otimes \exp\left(-\frac{i}{\hbar} \hat{H}_B(t - t')\right). \quad (\text{S-35})$$

From (S-33), we can evaluate  $\frac{d}{dt}\check{\rho}(t)$  using the transformation (S-34) and finally obtain the quantum Liouville–von Neumann equation in interaction picture as

$$\frac{d}{dt}\check{\rho}(t) = \frac{\lambda}{i\hbar} [\check{H}_{SB}(t), \check{\rho}(t)] = \lambda \check{\mathcal{L}}_{SB}(t) \check{\rho}(t), \quad (\text{S-36})$$

where  $\check{\mathcal{L}}$  is Liouville operator.

Because only system ( $S$ ) is our concern, all degrees of freedom related to the bath ( $B$ ) must be traced out

$$\frac{d}{dt}\check{\rho}_S(t) = \lambda \text{Tr}_B \check{\mathcal{L}}_{SB}(t) \check{\rho}(t). \quad (\text{S-37})$$

However, above equation does not give us a dynamical map form

$$\frac{d}{dt}\check{\rho}_S(t) = \lambda \mathcal{M}(t) \check{\rho}_S(t), \quad (\text{S-38})$$

due to the correlation between the system and the bath. Fortunately, in the weak coupling limit, we can obtain the dynamical map by some assumptions: (i) the initial state is separable  $\hat{\rho}(t_0) = \hat{\rho}_S(t_0) \otimes \hat{\rho}_B = \check{\rho}(t_0)$ , (ii) perturbed higher than second-order terms of interacting Hamiltonian  $\lambda^2$  are negligible, (iii) any trace consisting odd moments of  $\check{H}_{SB}(t)$  (or  $\check{B}(t)$ ) vanishes  $\text{Tr}_B \{\check{H}_{SB}(t_1) \check{H}_{SB}(t_2) \cdots \check{H}_{SB}(t_{2n+1}) \hat{\rho}_B\} = 0$ . Combining these assumptions and then considering full interacting case  $\lambda = 1$ , the quantum Liouville-von Neumann equation within weak coupling approximation is now in a dynamical map form [25]

$$\begin{aligned} \frac{d}{dt}\check{\rho}_S(t) &\approx -\frac{1}{\hbar^2} \int_0^{t-t_0} d\tau \text{Tr}_B [\check{\mathcal{H}}_{SB}(t), [\check{\mathcal{H}}_{SB}(t-\tau), \check{\rho}_S(t) \otimes \hat{\rho}_B]], \\ &\approx \frac{1}{\hbar^2} \sum_{\alpha, \beta} \int_0^{t-t_0} d\tau \{ \check{A}_\beta(t-\tau) \check{\rho}_S(t) \check{A}_\alpha^\dagger(t) - \check{A}_\alpha^\dagger(t) \check{A}_\beta(t-\tau) \check{\rho}_S(t) \} \text{Tr}_B [\check{B}_\alpha(t) \check{B}_\beta(t-\tau) \hat{\rho}_B] + \text{h.c.} \end{aligned} \quad (\text{S-39})$$

Here explicit form of  $\check{\mathcal{H}}_{SB}$  is given in (S-32) while  $\text{Tr}_B [\check{B}_\alpha(t) \check{B}_\beta(t-\tau) \hat{\rho}_B] = \text{Tr}_B [\check{B}_\beta(t-\tau) \hat{\rho}_B \check{B}_\alpha(t)]$ .

If **the bath is keeping in a steady state** i.e.  $[\hat{H}_B, \hat{\rho}_B] = 0$ . Meanwhile

$$\begin{aligned} \text{Tr}_B [\check{B}_\alpha(t) \check{B}_\beta(t-\tau) \hat{\rho}_B] &= \text{Tr}_B \left[ e^{-\frac{i}{\hbar} \hat{H}_B(t-t_0)} \hat{B} e^{\frac{i}{\hbar} \hat{H}_B(t-t_0)} e^{-\frac{i}{\hbar} \hat{H}_B(t-\tau-t_0)} \hat{B} e^{\frac{i}{\hbar} \hat{H}_B(t-\tau-t_0)} \hat{\rho}_B \right] \\ &= \text{Tr}_B \left[ e^{-\frac{i}{\hbar} \hat{H}_B(t-t_0)} \hat{B} e^{\frac{i}{\hbar} \hat{H}_B \tau} \hat{B} \hat{\rho}_B e^{\frac{i}{\hbar} \hat{H}_B(t-\tau-t_0)} \right] \\ &= \text{Tr}_B \left[ e^{\frac{i}{\hbar} \hat{H}_B(t-\tau-t_0)} e^{-\frac{i}{\hbar} \hat{H}_B(t-t_0)} \hat{B} e^{\frac{i}{\hbar} \hat{H}_B \tau} \hat{B} \hat{\rho}_B \right] = \text{Tr}_B \left[ e^{-\frac{i}{\hbar} \hat{H}_B \tau} \hat{B} e^{\frac{i}{\hbar} \hat{H}_B \tau} \hat{B} \hat{\rho}_B \right] \\ &= \text{Tr}_B [\check{B}_\alpha(\tau) \check{B}_\beta(0) \hat{\rho}_B] \equiv C_{\alpha\beta}(\tau), \end{aligned} \quad (\text{S-41})$$

is time independent and namely bath correlation function. The most common case is when  $\hat{\rho}_B = e^{-\hat{H}_B/k_B T} / \text{Tr}_B (e^{-\hat{H}_B/k_B T})$ .

Within this assumption, our dynamic equation becomes

$$\frac{d}{dt}\check{\rho}_S(t) = \frac{1}{\hbar^2} \sum_{\alpha, \beta} \int_0^{t-t_0} d\tau C_{\alpha\beta}(\tau) \{ \check{A}_\beta(t-\tau) \check{\rho}_S(t) \check{A}_\alpha^\dagger(t) - \check{A}_\alpha^\dagger(t) \check{A}_\beta(t-\tau) \check{\rho}_S(t) \} + \text{h.c.} \quad (\text{S-42})$$

Using inverse transformation of (S-34), we can rewrite equation (S-42) in Schrödinger picture

$$\begin{aligned}
\frac{d}{dt}\hat{\rho}_S(t) &= \frac{d}{dt}\hat{U}_S^\dagger(t, t_0)\check{\rho}_S(t)\hat{U}_S(t, t_0) = \frac{1}{i\hbar}\left[\hat{H}_S(t), \hat{\rho}_S(t)\right] + \hat{U}_S^\dagger(t, t_0)\frac{d}{dt}\check{\rho}_S(t)\hat{U}_S(t, t_0) \\
&= \frac{1}{i\hbar}\left[\hat{H}_S(t), \hat{\rho}_S(t)\right] + \frac{1}{\hbar^2}\sum_{\alpha, \beta}\int_0^{t-t_0}d\tau C_{\alpha\beta}(\tau)\hat{U}_S^\dagger(t, t_0)\left\{\check{A}_\beta(t-\tau)\check{\rho}_S(t)\check{A}_\alpha^\dagger(t) - \check{A}_\alpha^\dagger(t)\check{A}_\beta(t-\tau)\check{\rho}_S(t)\right\}\hat{U}_S(t, t_0) + \text{h.c.} \\
&= \frac{1}{i\hbar}\left[\hat{H}_S(t), \hat{\rho}_S(t)\right] + \left\{\frac{1}{\hbar^2}\sum_{\alpha, \beta}\int_0^{t-t_0}d\tau C_{\alpha\beta}(\tau)\left\{\hat{U}_S(t, t-\tau)\hat{A}_\beta(t-\tau)\hat{U}_S^\dagger(t, t-\tau)\right\}\hat{\rho}_S(t)\hat{A}_\alpha^\dagger(t) \right. \\
&\quad \left. - \frac{1}{\hbar^2}\sum_{\alpha, \beta}\hat{A}_\alpha^\dagger(t)\left\{\int_0^{t-t_0}d\tau C_{\alpha\beta}(\tau)\hat{U}_S(t, t-\tau)\hat{A}_\beta(t-\tau)\hat{U}_S^\dagger(t, t-\tau)\right\}\hat{\rho}_S(t) + \text{h.c.}\right\}. \tag{S-43}
\end{aligned}$$

Defining the bath-convoluted operator

$$\hat{S}_\alpha(t) = \frac{1}{\hbar^2}\sum_{\beta}\int_0^{t-t_0}d\tau C_{\alpha\beta}(\tau)\hat{U}_S(t, t-\tau)\hat{A}_\beta(t-\tau)\hat{U}_S^\dagger(t, t-\tau), \tag{S-44}$$

then the quantum master equation in Schrödinger picture reads

$$\frac{d}{dt}\hat{\rho}_S(t) = \frac{1}{i\hbar}\left[\hat{H}_S(t), \hat{\rho}_S(t)\right] - \left\{\sum_{\alpha}\left[\hat{A}_\alpha(t), \hat{S}_\alpha(t)\hat{\rho}_S(t)\right] + \text{h.c.}\right\}. \tag{S-45}$$

When the interaction between the bath and system is time-independent  $\hat{A}_\alpha(t) = \hat{A}_\alpha$  and the spectra of  $\hat{H}_S(t)$  is known

$$\hat{H}_S(t)|k(t)\rangle = E_k(t)|k(t)\rangle, \tag{S-46}$$

we can define spectral decomposition of  $\hat{A}_\alpha$  as

$$\hat{A}_\alpha = \sum_{m, n} \langle n(t) | \hat{A}_\alpha | m(t) \rangle | n(t) \rangle \langle m(t) |. \tag{S-47}$$

Then the bath-convoluted operator  $\hat{S}_\alpha(t)$  becomes

$$\hat{S}_\alpha(t) = \sum_{m, n} \langle n(t) | \hat{A}_\alpha | m(t) \rangle \frac{1}{\hbar^2} \sum_{\beta} \int_0^{t-t_0} d\tau C_{\alpha\beta}(\tau) \hat{U}_S(t, t-\tau) | n(t) \rangle \langle m(t) | \hat{U}_S^\dagger(t, t-\tau). \tag{S-48}$$

Now we need to compare between time scale of the system ( $S$ ) and the bath ( $B$ ) to employ more approximation. The time evolution of the system is characterized by temporal time scale of eigenenergy and eigenstate

$$\tau_E^{-1} = \max_n \left| \frac{1}{E_m(t)} \frac{dE_m(t)}{dt} \right| \tag{S-49}$$

$$\tau_s^{-1} = \max_{m \neq n} \left| \left\langle m(t) \left| \frac{d}{dt} \right| n(t) \right\rangle \right|, \tag{S-50}$$

then the temporal time scale for system ( $S$ ) is the lowest one  $\tau_S = \min(\tau_E, \tau_s)$ . On the other hand, the bath correlation function  $C_{\alpha\beta}(\tau)$  decays with the time scale  $\tau_{B, \alpha, \beta}$ . Therefore, the global decay time scale for the bath correlation function should be  $\tau_B = \max_{\alpha, \beta} \tau_{B, \alpha, \beta}$ . If  $\tau_B \ll t - t_0$ , the bath-convoluted operator becomes the Markovian one or we have **the Born-Markov approximation** [25]

$$\hat{S}_\alpha(t) \approx \sum_{m, n} \langle n(t) | \hat{A}_\alpha | m(t) \rangle \frac{1}{\hbar^2} \sum_{\beta} \int_0^{+\infty} d\tau C_{\alpha\beta}(\tau) \hat{U}_S(t, t-\tau) | n(t) \rangle \langle m(t) | \hat{U}_S^\dagger(t, t-\tau). \tag{S-51}$$

Suppose the bath correlation function  $C_{\alpha\beta}(\tau)$  decays faster than the evolution of the system  $\tau_B \ll \tau_A$ , then

$$\hat{U}_S(t, t-\tau) \approx e^{-\frac{i}{\hbar}\hat{H}_S(t)\tau} \tag{S-52}$$

and consequently, the bath convoluted operator becomes

$$\begin{aligned}
\hat{S}_\alpha(t) &\approx \sum_{m,n} \langle n(t) | \hat{A}_\alpha | m(t) \rangle \frac{1}{\hbar^2} \sum_\beta \int_0^{+\infty} d\tau C_{\alpha\beta}(\tau) e^{-\frac{i}{\hbar} \hat{H}_S(t)\tau} |n(t)\rangle \langle m(t)| e^{\frac{i}{\hbar} \hat{H}_S(t)\tau} \\
&= \sum_{m,n} \langle n(t) | \hat{A}_\alpha | m(t) \rangle \frac{1}{\hbar^2} \sum_\beta \int_0^{+\infty} d\tau C_{\alpha\beta}(\tau) e^{\frac{i}{\hbar} (E_m - E_n)\tau} |n(t)\rangle \langle m(t)| \\
&= \sum_{m,n} \langle n(t) | \hat{A}_\alpha | m(t) \rangle \frac{1}{\hbar^2} \sum_\beta \Gamma_{\alpha\beta} (E_m - E_n) |n(t)\rangle \langle m(t)|,
\end{aligned} \tag{S-53}$$

where  $\Gamma(E)_{\alpha\beta}$  is bath-induced transition rate [25]

$$\Gamma_{\alpha\beta}(E) = \int_0^{+\infty} d\tau C_{\alpha\beta}(\tau) e^{\frac{i}{\hbar} (E+i0^+)\tau}. \tag{S-54}$$

Corresponding, we have the bath-induced relaxation time scale

$$\tau_R^{-1} = \max_{\alpha,\beta,E} \Gamma_{\alpha\beta}(E). \tag{S-55}$$

Our Born-Markov approximation is valid if  $\tau_B \ll \tau_R$  too [25].

## 2. Caldeira–Leggett model of thermal harmonic bath

The Caldeira–Leggett or harmonic bath model is commonly used to demonstrate the quantum dissipation [33, 34]

$$\hat{H}_{int+B} = \sum_i \left[ \frac{\hat{p}_i^2}{2m_i} + \frac{1}{2} m_i \omega_i^2 \left( \hat{x}_i - \frac{c_i}{m_i \omega_i^2} \mathcal{F}(\hat{x}) \right)^2 \right], \tag{S-56}$$

where the choice of  $\mathcal{F}(\hat{x})$  strongly depends on the global symmetry of the system's Hamiltonian  $\hat{H}_S$ . The bath is characterized by the following spectral function

$$J(\omega) = \hbar \sum_i \frac{c_i^2}{2m_i \omega_i} \delta(\omega - \omega_i), \quad J(-\omega) = -J(\omega), \tag{S-57}$$

where  $\alpha$  represents the strength of the system-bath interaction while the cutoff  $\omega_c$  separates the Ohmic low-frequency regime from the decay high-frequency regime. Notice that if  $\alpha = 0$ , then  $J(\omega) = 0$  for all frequencies and  $c_i = 0$  i.e. there is no coupling between the system and the bath  $\hat{H}_{int} = 0$ . Moreover, the following trick is useful for further calculations

$$\hbar \sum_i \frac{c_i^2}{2m_i \omega_i} f(\omega_i) = \hbar \sum_i \frac{c_i^2}{2m_i \omega_i} \int_0^{+\infty} f(\omega) \delta(\omega - \omega_i) d\omega = \int_0^{+\infty} J(\omega) f(\omega) d\omega. \tag{S-58}$$

The whole Hamiltonian can be written explicitly as

$$\hat{H}(t) = \hat{H}_S(t) + \hat{H}_{int+B} = \hat{H}'_S(t) + \hat{A} \otimes \hat{B} + \hat{H}_B, \tag{S-59}$$

where

$$\hat{H}'_S(t) = \hat{H}_S(t) + \left( \sum_i \frac{c_i^2}{2m_i \omega_i^2} \right) \mathcal{F}^2(\hat{x}) = \hat{H}_S(t) + u_{rn} \mathcal{F}^2(\hat{x}) \tag{S-60}$$

$$\hat{A} \otimes \hat{B} = \mathcal{F}(\hat{x}) \otimes \left[ - \sum_i c_i \hat{x}_i \right] \tag{S-61}$$

$$\hat{H}_B = \sum_i \left( \frac{\hat{p}_i^2}{2m_i} + \frac{1}{2} m_i \omega_i^2 \hat{x}_i^2 \right), \tag{S-62}$$



where renormalization potential amplitude  $u_{rn}$  is obtained by using the trick (S-58) for  $f(\omega) = \frac{1}{\omega}$  to get

$$u_{rn} = \sum_i \frac{c_i^2}{2m_i\omega_i^2} = \sum_i \frac{c_i^2}{2m_i\omega_i} \int_0^\infty \frac{1}{\omega} \delta(\omega - \omega_i) d\omega = \frac{1}{\hbar} \int_0^{+\infty} \frac{1}{\omega} J(\omega) d\omega. \quad (\text{S-63})$$

The bath Hamiltonian can be diagonalized as

$$\hat{H}_B = \sum_i \hat{h}_i = \sum_i \left( n_i + \frac{1}{2} \right) \hbar\omega_i |n_i\rangle \langle n_i|, \quad (\text{S-64})$$

and matrix element of displacement is

$$\langle n_i | \hat{x}_i | m_i \rangle = \sqrt{\frac{\hbar}{2m_i\omega_i}} (\sqrt{n_i} \delta_{n_i, m_i+1} + \sqrt{m_i} \delta_{n_i+1, m_i}). \quad (\text{S-65})$$

The bath correlation function when it stays at the thermal equilibrium state  $\hat{\rho}_B = e^{-\hat{H}_B/k_B T} / \text{Tr}_B (e^{-\hat{H}_B/k_B T})$

$$\begin{aligned} C(\tau) &= \text{Tr}_B [\check{B}(\tau) \check{B}(0) \hat{\rho}_B] = \sum_j c_j^2 \frac{\text{Tr}_B [e^{-\frac{i}{\hbar} \hat{h}_j t} \hat{x}_j e^{\frac{i}{\hbar} \hat{h}_j t} \hat{x}_j e^{-\hat{h}_j/k_B T}]}{\text{Tr}_B e^{-\hat{h}_j/k_B T}} + \sum_{j \neq k} c_j c_k \frac{\text{Tr}_B [e^{-\frac{i}{\hbar} \hat{h}_k t} \hat{x}_k e^{\frac{i}{\hbar} \hat{h}_k t} \hat{x}_j e^{-\hat{h}_k/k_B T} e^{-\hat{h}_j/k_B T}]}{\text{Tr}_B e^{-\hat{h}_k/k_B T} e^{-\hat{h}_j/k_B T}} \\ &= \sum_j c_j^2 \frac{\text{Tr}_B [e^{-\frac{i}{\hbar} \hat{h}_j t} \hat{x}_j e^{\frac{i}{\hbar} \hat{h}_j t} \hat{x}_j e^{-\hat{h}_j/k_B T}]}{\text{Tr}_B e^{-\hat{h}_j/k_B T}} + \sum_{j \neq k} c_j c_k \frac{\text{Tr}_B [e^{-\frac{i}{\hbar} \hat{h}_k t} \hat{x}_k e^{\frac{i}{\hbar} \hat{h}_k t} e^{-\hat{h}_k/k_B T}]}{\text{Tr}_B e^{-\hat{h}_k/k_B T}} \frac{\text{Tr}_B [\hat{x}_j e^{-\hat{h}_j/k_B T}]}{\text{Tr}_B e^{-\hat{h}_j/k_B T}} \\ &= \sum_j c_j^2 \frac{\sum_{n,m} [e^{-i(n+1/2)\omega t} \langle n | \hat{x}_j | m \rangle e^{i(m+1/2)\omega t} \langle m | \hat{x}_j | n \rangle e^{-n\hbar\omega_j/k_B T}]}{\sum_n e^{-n\hbar\omega_j/k_B T}} \\ &= \sum_j c_j^2 \frac{\sum_{n,m} [\langle n | \hat{x}_j | m \rangle \langle m | \hat{x}_j | n \rangle e^{-i(n-m)\omega t} e^{-n\hbar\omega_j/k_B T}]}{\sum_n e^{-n\hbar\omega_j/k_B T}} \\ &= \hbar \sum_j \frac{c_j^2}{2m_j\omega_j} \left[ e^{i\omega_j\tau} \frac{\sum_n n e^{-n\hbar\omega_j/k_B T}}{\sum_n e^{-n\hbar\omega_j/k_B T}} + e^{-i\omega_j\tau} \frac{\sum_n (n+1) e^{-n\hbar\omega_j/k_B T}}{\sum_n e^{-n\hbar\omega_j/k_B T}} \right] \\ &= \hbar \sum_j \frac{c_j^2}{2m_j\omega_j} [e^{i\omega_j\tau} f_{BE}(\omega_j) + e^{-i\omega_j\tau} [f_{BE}(\omega_j) + 1]] \\ &= \hbar \sum_j \frac{c_j^2}{2m_j\omega_j} \int_0^{+\infty} [e^{i\omega\tau} f_{BE}(\omega) + e^{-i\omega\tau} [f_{BE}(\omega) + 1]] \delta(\omega - \omega_j) d\omega \\ &= \int_0^{+\infty} J(\omega) [e^{i\omega\tau} f_{BE}(\omega) + e^{-i\omega\tau} [f_{BE}(\omega) + 1]] d\omega \\ &= \int_{-\infty}^{+\infty} e^{i\omega\tau} f_{BE}(\omega) J(\omega) d\omega, \end{aligned} \quad (\text{S-66})$$

where Bose-Einstein distribution

$$f_{BE}(\omega) = \frac{\sum_n n e^{-n\hbar\omega/k_B T}}{\sum_n e^{-n\hbar\omega/k_B T}} = \frac{1}{e^{\hbar\omega/k_B T} - 1}, \quad f_{BE}(\omega) + 1 = -f_{BE}(-\omega) \quad (\text{S-67})$$

The corresponding bath-induced transition rate can also be calculated

$$\begin{aligned} \Gamma(E) &= \int_0^{+\infty} d\tau C(\tau) e^{\frac{i}{\hbar}(E+i0^+)\tau} = \int_{-\infty}^{+\infty} d\omega J(\omega) f_{BE}(\omega) \int_0^{+\infty} e^{i(\omega+E/\hbar+i0^+)\tau} d\tau \\ &= \int_{-\infty}^{+\infty} d\omega \left( -\pi \delta\left(\omega + \frac{E}{\hbar}\right) + i\mathcal{P} \frac{1}{\omega + \frac{E}{\hbar}} \right) J(\omega) f_{BE}(\omega) \\ &= \pi J\left(\frac{E}{\hbar}\right) \left[ f_{BE}\left(\frac{E}{\hbar}\right) + 1 \right] + i\mathcal{P} \int_{-\infty}^{+\infty} \frac{J(\omega) f_{BE}(\omega) \hbar d\omega}{E + \hbar\omega}, \end{aligned} \quad (\text{S-68})$$

or

$$\gamma(E) = 2\Re\Gamma(E) = 2\pi J\left(\frac{E}{\hbar}\right) \left[ f_{BE}\left(\frac{E}{\hbar}\right) + 1 \right], \quad (\text{S-69})$$

$$\begin{aligned} \sigma(E) = \Im\Gamma(E) &= \mathcal{P} \int_{-\infty}^{+\infty} \frac{J(\omega) f_{BE}(\omega) \hbar d\omega}{E + \hbar\omega} \\ &= -\mathcal{P} \int_0^{+\infty} \frac{J(\omega)}{\omega} d\omega + E \left\{ \mathcal{P} \int_0^{+\infty} \frac{J(\omega)}{\hbar\omega(E - \hbar\omega)} \hbar d\omega + \mathcal{P} \int_0^{+\infty} \frac{2J(\omega)}{E^2 - \hbar^2\omega^2} f_{BE}(\omega) \hbar d\omega \right\} \\ &= -\hbar u_{rn} + E \left\{ \mathcal{P} \int_0^{+\infty} \frac{J(\xi/\hbar)}{\xi(E - \xi)} d\xi + \mathcal{P} \int_0^{+\infty} \frac{2J(\xi/\hbar)}{E^2 - \xi^2} f_{BE}(\xi/\hbar) d\xi \right\}. \end{aligned} \quad (\text{S-70})$$

At Ohmic damping limit

$$J(\omega) = 2\hbar^2 \alpha \omega e^{-|\omega|/\omega_c}. \quad (\text{S-71})$$

Then Eq. (S-63) becomes

$$u_{rn} = \frac{1}{\hbar} \int_0^{+\infty} \frac{1}{\omega} J(\omega) d\omega = 2\alpha \hbar \int_0^{+\infty} e^{-\omega/\omega_c} d\omega = 2\alpha \hbar \omega_c. \quad (\text{S-72})$$

The bath correlation function at Ohmic damping limit is found as

$$C(\tau) = 2\alpha k_B^2 T^2 \left[ \zeta\left(2, 1 + \frac{k_B T}{\hbar\omega_c} (1 - i\omega_c \tau)\right) + \zeta\left(2, \frac{k_B T}{\hbar\omega_c} (1 - i\omega_c \tau)\right) \right], \quad (\text{S-73})$$

where  $\zeta(s, z) = \sum_{k=0}^{\infty} [(k+z)^2]^{-s/2}$  is Hurwitz zeta function. The real and image parts of the transition rate are explicitly found as

$$\gamma(E) = 2\Re\Gamma(E) = \frac{4\pi\hbar\alpha E e^{-|E|/\hbar\omega_c}}{1 - e^{-E/k_B T}}, \quad (\text{S-74})$$

and

$$\sigma(E) = \Im\Gamma(E) = 2\hbar\alpha \left\{ -\hbar\omega_c + E \left[ \sum_{n=0}^{\infty} e^{-\frac{E}{\hbar\omega_c} - \frac{nE}{k_B T}} \text{Ei}\left(\frac{E}{\hbar\omega_c} + \frac{nE}{k_B T}\right) + \sum_{n=1}^{\infty} e^{\frac{E}{\hbar\omega_c} + \frac{nE}{k_B T}} \text{Ei}\left(-\frac{E}{\hbar\omega_c} - \frac{nE}{k_B T}\right) \right] \right\} \quad (\text{S-75})$$

Here  $\text{Ei}(z)$  is exponential integral function.

### 3. Choice of $\mathcal{F}(\hat{x})$ and Matrix representations in the basis set of moving harmonic oscillator $|n^{(0)}(\bar{t})\rangle$

The Hamiltonian of the system  $\hat{H}_S$  can be re-written in another form,

$$\hat{H}_S(t) = -\frac{1}{2} \frac{\partial^2}{\partial \bar{x}^2} + \frac{1}{2} (\bar{x} - \bar{v}\bar{t})^2 + \frac{1}{2} u_0 - \frac{1}{2} u_0 \cos\left(\frac{2\pi\ell}{a} \bar{x}\right), \quad (\text{S-76})$$

in order to illustrate its periodicity of  $(\frac{2\pi\ell}{a} \bar{x})$ . Then it is obvious to choose  $\mathcal{F}(\hat{x})$  as a smooth periodic function of  $(\frac{2\pi\ell}{a} \bar{x})$ . At  $\bar{t} = 0$ , the global minimum of the potential surface is at  $\bar{x} = 0$ , therefore, the most natural choice is  $\mathcal{F}(\hat{x}) = \sin(\frac{2\pi\ell}{a} \bar{x})$ .

With this choice of  $\mathcal{F}(\hat{x})$ , we indicate that  $\hat{A} = \mathcal{F}(\hat{x}) = \sin(\frac{2\pi\ell}{a} \bar{x})$  and then the quantum Liouville - von Neumann master equation for the density matrix is written as [25]

$$\frac{d}{d\bar{t}} \hat{\rho}_S(\bar{t}) = -i \left[ \hat{H}_S(\bar{t}) + 2\alpha\omega_c \hat{A}^2, \hat{\rho}_S(\bar{t}) \right] - \left\{ \left[ \hat{A}, \hat{S}(\bar{t}) \hat{\rho}_S(\bar{t}) \right] + \text{Hermitian conjugate} \right\}, \quad (\text{S-77})$$

where  $\hat{S}(t) \approx \sum_{m,n} \langle n(\bar{t}) | \hat{A} | m(\bar{t}) \rangle \Gamma(E_m - E_n) |n(\bar{t})\rangle \langle m(\bar{t})|$ .

Let us define the bath-induced transition matrix whose elements are defined as

$$\Gamma_{m,m'}(\bar{t}) = \Gamma [E_{m'}(\bar{t}) - E_m(\bar{t})], \quad (\text{S-78})$$

where  $E_m(\bar{t})$  is quasistatic eigenvalue of system's Hamiltonian  $\hat{H}_S(\bar{t})$ .

In the basis of  $|n^{(0)}(\bar{t})\rangle$ , matrix representation of operator  $\hat{A} = \sin\left(\frac{2\pi}{a}\hat{x}\right)$ , or  $\hat{A} = \sin\left(\frac{2\pi\ell}{a}\bar{v}\bar{t}\right) \cos\left(\frac{2\pi\ell}{a}(\bar{x} - \bar{v}\bar{t})\right) + \cos\left(\frac{2\pi\ell}{a}\bar{v}\bar{t}\right) \sin\left(\frac{2\pi\ell}{a}(\bar{x} - \bar{v}\bar{t})\right)$ , is found as

$$\begin{aligned} A_{n,n'}(\bar{t}) &= \left\langle n^{(0)}(\bar{t}) \left| \sin\left(\frac{2\pi\ell}{a}\bar{x}\right) \right| n'^{(0)}(\bar{t}) \right\rangle \\ &= 2 \sin\left(\frac{2\pi\ell}{a}\bar{v}\bar{t}\right) I_{n,n'} + 2 \cos\left(\frac{2\pi\ell}{a}\bar{v}\bar{t}\right) J_{n,n'}, \end{aligned} \quad (\text{S-79})$$

where the integrals  $I, J$  are given in Eqs. (S-9)-(S-10). Meanwhile the one of the bath convoluted operator is also found

$$\begin{aligned} S_{n,n'}(\bar{t}) &= \left\langle n^{(0)}(\bar{t}) \left| \hat{S}(\bar{t}) \right| n'^{(0)}(\bar{t}) \right\rangle \\ &= \sum_{m,m'} \left\langle n^{(0)}(\bar{t}) \left| m(\bar{t}) \right\rangle \left\langle m(\bar{t}) \left| \hat{A} \right| m'(\bar{t}) \right\rangle \Gamma_{m,m'} \left\langle m'(\bar{t}) \left| n'^{(0)}(\bar{t}) \right\rangle \right. \\ &= \sum_{m,m',k,k'} \left\langle n^{(0)}(\bar{t}) \left| m(\bar{t}) \right\rangle \left\langle m(\bar{t}) \left| k^{(0)}(\bar{t}) \right\rangle A_{k,k'}(\bar{t}) \left\langle k'^{(0)}(\bar{t}) \left| m'(\bar{t}) \right\rangle \Gamma_{m,m'} \left\langle m'(\bar{t}) \left| n'^{(0)}(\bar{t}) \right\rangle \right. \\ &= \sum_{m,m',k,k'} c_{m,n}(\bar{t}) c_{m,k}^*(\bar{t}) A_{k,k'}(\bar{t}) c_{m',k'}(\bar{t}) \Gamma_{m,m'} c_{m',n'}^*(\bar{t}) \\ &= \{c^T \cdot [(c^* \cdot A \cdot c^T) \odot \Gamma] \cdot c^*\}_{n,n'}. \end{aligned} \quad (\text{S-80})$$

Here  $\cdot$  stands for normal matrix multiplication while  $\odot$  stands for Hadamard (or Schur) product. Such representation is useful in matrix calculations.

Similar to Eq. (S-23), the matrix representation of the quantum master equation (S-45) reads

$$\frac{d}{dt} \rho_S(\bar{t}) = -i [H_S(\bar{t}) + 2\alpha\omega_c A^2(\bar{t}) - \sigma_t(\bar{t}), \rho_S(\bar{t})] - \{[A(\bar{t}), S(\bar{t})\rho_S(\bar{t})] + \text{h.c.}\}. \quad (\text{S-81})$$

Above ordinary differential equation of matrix can also be solve by forth order Runge-Kutta method

$$\begin{aligned} \rho_S(\bar{t} + \Delta\bar{t}) &= \rho_S(\bar{t}) + \frac{1}{6} (\kappa_1 + 2\kappa_2 + 2\kappa_3 + \kappa_4) \Delta\bar{t}, \quad (\text{S-82}) \\ \left\{ \begin{array}{l} \kappa_1 = -i [H_S(\bar{t}) + 2\alpha\omega_c A^2(\bar{t}) - \sigma_t, \rho_S(\bar{t})] - \{[A(\bar{t}), S(\bar{t})\rho_S(\bar{t})] + \text{h.c.}\} \\ \kappa_2 = -i [H_S(\bar{t} + \frac{1}{2}\Delta\bar{t}) + 2\alpha\omega_c A^2(\bar{t} + \frac{1}{2}\Delta\bar{t}) - \sigma_t, \rho_S(\bar{t}) + \frac{1}{2}\kappa_1 \Delta\bar{t}] - \{[A(\bar{t} + \frac{1}{2}\Delta\bar{t}), S(\bar{t} + \frac{1}{2}\Delta\bar{t}) (\rho_S(\bar{t}) + \frac{1}{2}\kappa_1 \Delta\bar{t})] + \text{h.c.}\} \\ \kappa_3 = -i [H_S(\bar{t} + \frac{1}{2}\Delta\bar{t}) + 2\alpha\omega_c A^2(\bar{t} + \frac{1}{2}\Delta\bar{t}) - \sigma_t, \rho_S(\bar{t}) + \frac{1}{2}\kappa_2 \Delta\bar{t}] - \{[A(\bar{t} + \frac{1}{2}\Delta\bar{t}), S(\bar{t} + \frac{1}{2}\Delta\bar{t}) (\rho_S(\bar{t}) + \frac{1}{2}\kappa_2 \Delta\bar{t})] + \text{h.c.}\} \\ \kappa_4 = -i [H_S(\bar{t} + \Delta\bar{t}) + 2\alpha\omega_c A^2(\bar{t} + \Delta\bar{t}) - \sigma_t, \rho_S(\bar{t}) + \kappa_3 \Delta\bar{t}] - \{[A(\bar{t} + \Delta\bar{t}), S(\bar{t} + \Delta\bar{t}) (\rho_S(\bar{t}) + \kappa_3 \Delta\bar{t})] + \text{h.c.}\} \end{array} \right. \end{aligned}$$

## S-XI. CLASSICAL DYNAMICAL EVOLUTION WITH ENVIROMENT: THE CASE OF CALDEIRA-LEGGETT MODEL

In order to emphasize on quantum effects in our system, we also examine the classical motion whose dynamics is governed by stochastic Newton second law. Starting from the Hamiltonian (10) in the manuscript, the Hamilton equations for the whole system including harmonic bath are given as [34]

$$\left\{ \begin{array}{l} \frac{d^2\bar{x}}{d\bar{t}^2} + (\bar{x} - \bar{v}\bar{t}) + \frac{u_0\pi\ell}{a} \sin\left(\frac{2\pi\ell}{a}\bar{x}\right) = f_{bath}(\bar{x}, \bar{t}), \\ \frac{d^2x_i}{d\bar{t}^2} + \omega_i^2 x_i = \frac{c_i}{m_i} \sin\left(\frac{2\pi\ell}{a}\bar{x}\right), \end{array} \right. \quad (\text{S-83})$$

where the force coming from the harmonic bath is

$$f_{bath}(\bar{x}, \bar{t}) = \frac{2\pi\ell}{a} \left( \sum_i x_i c_i \right) \cos\left(\frac{2\pi\ell}{a}\bar{x}\right) - \frac{2\pi\ell}{a} \left( \sum_i \frac{c_i^2}{2m_i\omega_i^2} \right) \sin\left(\frac{4\pi\ell}{a}\bar{x}\right). \quad (\text{S-84})$$

Now we need to solve for the dynamical evolution of the bath degrees of freedom  $x_i$  in order to determine the bath force. Because the Green function of the harmonic bath is known as  $G(\bar{t}, \bar{t}') = \frac{1}{\omega_i} \Theta(\bar{t} - \bar{t}') \sin[\omega_i(\bar{t} - \bar{t}')] ]$ , the dynamical equation for the degree of freedom of the heat bath can be easily solved

$$x_i(\bar{t}) = x_i^{homo}(\bar{t}) + \frac{c_i}{m_i \omega_i} \int_0^{\bar{t}} \sin\left[\frac{2\pi\ell}{a} \bar{x}(\bar{t}')\right] \sin[\omega_i(\bar{t} - \bar{t}')] d\bar{t}' \quad (\text{S-85})$$

where the homogeneous solution is determined via initial positions and velocities of bath oscillators  $x_i(0), v_i(0)$  as  $x_i^{homo}(\bar{t}) = x_i(0) \cos(\omega_i \bar{t}) + \frac{v_i(0)}{\omega_i} \sin(\omega_i \bar{t})$ . Integrating by part the second term of Eq. (S-85) gives us

$$x_i(\bar{t}) = x_i^{homo}(\bar{t}) + \frac{c_i}{m_i \omega_i^2} \sin\left[\frac{2\pi\ell}{a} \bar{x}(\bar{t})\right] - \frac{c_i}{m_i \omega_i^2} \cos(\omega_i \bar{t}) \sin\left[\frac{2\pi\ell}{a} \bar{x}(0)\right] - \frac{2\pi\ell}{a} \frac{c_i}{m_i \omega_i^2} \int_0^{\bar{t}} \cos[\omega_i(\bar{t} - \bar{t}')] \cos\left[\frac{2\pi\ell}{a} \bar{x}(\bar{t}')\right] \frac{d\bar{x}(\bar{t}')}{d\bar{t}'} d\bar{t}'. \quad (\text{S-86})$$

As  $x_i(\bar{t})$  is found, the force coming from harmonic bath is simplified as

$$f_{bath}[\bar{x}(\bar{t}), \bar{t}] = \frac{2\pi\ell}{a} \left\{ \sum_i c_i \left[ x_i^{homo}(\bar{t}) - \sum_i \frac{c_i}{m_i \omega_i^2} \sin\left[\frac{2\pi\ell}{a} \bar{x}(0)\right] \cos(\omega_i \bar{t}) \right] \right\} \cos\left[\frac{2\pi\ell}{a} \bar{x}(\bar{t})\right] - \frac{4\pi^2 \ell^2}{a^2} \cos\left[\frac{2\pi\ell}{a} \bar{x}(\bar{t})\right] \int_0^{\bar{t}} \left[ \sum_i \frac{c_i^2}{m_i \omega_i^2} \cos[\omega_i(\bar{t} - \bar{t}')] \right] \cos\left[\frac{2\pi\ell}{a} \bar{x}(\bar{t}')\right] \frac{d\bar{x}(\bar{t}')}{d\bar{t}'} d\bar{t}'. \quad (\text{S-87})$$

The summation over bath degrees of freedom appeared in the second term can be rewritten in term of spectral function  $J(\omega) = \sum_i \frac{c_i^2}{2m_i \omega_i} \delta(\omega - \omega_i) = 2\alpha\omega e^{-|\omega|/\omega_c}$ . Such terms are known as classical damping factor [34]:

$$\begin{aligned} \bar{\gamma}(\bar{t}) &= \sum_i \frac{c_i^2}{m_i \omega_i^2} \cos(\omega_i \bar{t}) = \int_0^{+\infty} \sum_i \frac{2 \cos(\omega_i \bar{t})}{\omega_i} \frac{c_i^2}{2m_i \omega_i} \delta(\omega - \omega_i) d\omega \\ &= \int_0^{+\infty} \frac{2 \cos(\omega \bar{t})}{\omega} \sum_i \frac{c_i^2}{2m_i \omega_i} \delta(\omega - \omega_i) d\omega = \int_0^{+\infty} \frac{2 \cos(\omega \bar{t})}{\omega} J(\omega) d\omega = \frac{4\alpha\omega_c}{1 + \omega_c^2 \bar{t}^2} \xrightarrow{\omega_c \rightarrow \infty} 4\pi\alpha\delta(\bar{t}). \end{aligned} \quad (\text{S-88})$$

Noticeably, the second term of the bath force depends on the velocity of the particle  $\frac{d\bar{x}}{d\bar{t}}$  and does not depends on the initial conditions of the bath degrees of freedom, therefore, can be interpreted as environmental viscous force [34]. On the other hand, the first term of the bath force, which is in {...} bracket depends on the initial conditions of both bath degrees of freedom  $x_i(0), v_i(0)$  and of particle  $\bar{x}(0)$  which will be pointed out as random force due to dissipation [34]. Thus, the bath force (S-87) is separated into viscous and random force  $f_{bath}[\bar{x}(\bar{t}), \bar{t}] = f_{vis}\left[\bar{x}, \frac{d\bar{x}}{d\bar{t}}\right] + f_{ran}(\bar{t})$  where

$$f_{vis}\left[\bar{x}, \frac{d\bar{x}}{d\bar{t}}\right] = -\frac{4\pi^2 \ell^2}{a^2} \cos\left[\frac{2\pi\ell}{a} \bar{x}(\bar{t})\right] \int_0^{\bar{t}} \bar{\gamma}(\bar{t} - \bar{t}') \cos\left[\frac{2\pi\ell}{a} \bar{x}(\bar{t}')\right] \frac{d\bar{x}(\bar{t}')}{d\bar{t}'} d\bar{t}' = -\frac{8\alpha\pi^3 \ell^2}{a^2} \cos^2\left(\frac{2\pi\ell}{a} \bar{x}\right) \frac{d\bar{x}}{d\bar{t}}, \quad (\text{S-89})$$

$$f_{ran}(\bar{t}) = \frac{2\pi\ell}{a} \left\{ \sum_i c_i \left[ x_i^{homo}(\bar{t}) - \sum_i \frac{c_i}{m_i \omega_i^2} \sin\left[\frac{2\pi\ell}{a} \bar{x}(0)\right] \cos(\omega_i \bar{t}) \right] \right\} \cos\left[\frac{2\pi\ell}{a} \bar{x}(\bar{t})\right]. \quad (\text{S-90})$$

Unlike viscous force, the random force depends on initial configuration of the bath degrees of freedom  $x_i(0), v_i(0)$ . Statistically, if the bath is kept at thermal equilibrium state obeying canonical Maxwell-Boltzmann distribution [34]

$$\rho_{bath} = Z^{-1} \exp\left\{ -k_B^{-1} T^{-1} \sum_i \left[ \frac{m_i v_i^2(0)}{2} + \frac{m_i \omega_i^2}{2} \left( x_i(0) - \frac{c_i}{m_i \omega_i^2} \sin\left(\frac{2\pi\ell}{a} \bar{x}(0)\right) \right) \right] \right\}, \quad (\text{S-91})$$

we can show that the statistics of random force is governed by the following relation [34]

$$\begin{aligned}
\langle f_{ran}(\bar{t}) \rangle &= 0, \\
\langle f_{ran}(\bar{t}) f_{ran}(\bar{t}') \rangle &= k_B T \frac{4\pi^2 \ell^2}{a^2} \cos \left[ \frac{2\pi\ell}{a} \bar{x}(\bar{t}) \right] \cos \left[ \frac{2\pi\ell}{a} \bar{x}(\bar{t}') \right] \sum_i \frac{c_i^2}{m_i \omega_i^2} \cos(\omega_i \bar{t}) \cos(\omega_i \bar{t}') \\
&= k_B T \frac{4\pi^2 \ell^2}{a^2} \cos \left[ \frac{2\pi\ell}{a} \bar{x}(\bar{t}) \right] \cos \left[ \frac{2\pi\ell}{a} \bar{x}(\bar{t}') \right] \sum_i \frac{c_i^2}{m_i \omega_i^2} \frac{1}{2} \left[ \cos(\omega_i(\bar{t} - \bar{t}')) + \cos(\omega_i(\bar{t} + \bar{t}')) \right] \\
&= k_B T \frac{2\pi^2 \ell^2}{a^2} \cos \left[ \frac{2\pi\ell}{a} \bar{x}(\bar{t}) \right] \cos \left[ \frac{2\pi\ell}{a} \bar{x}(\bar{t}') \right] \left[ \gamma(\bar{t} - \bar{t}') + \gamma(\bar{t} + \bar{t}') \right] \\
&= k_B T \frac{8\alpha\pi^3 \ell^2}{a^3} \cos^2 \left[ \frac{2\pi\ell}{a} \bar{x}(\bar{t}) \right] \delta(\bar{t} - \bar{t}').
\end{aligned} \tag{S-92}$$

This indicates that the random force obeys fluctuation-dissipation theorem because it originally comes from the thermal fluctuation of the harmonic bath [42].

Finally the motion of the driven particle is governed by the following stochastic Newton second law

$$\begin{cases} \frac{d\bar{x}}{d\bar{t}} = \dot{\bar{x}} \\ \frac{d\dot{\bar{x}}}{d\bar{t}} = -(\bar{x} - \bar{v}\bar{t}) - \frac{u_0\pi\ell}{a} \sin \left( \frac{2\pi\ell}{a} \bar{x} \right) - \frac{8\alpha\pi^3 \ell^2}{a^2} \cos^2 \left( \frac{2\pi\ell}{a} \bar{x} \right) \dot{\bar{x}} + f_{ran}(\bar{t}), \end{cases}, \tag{S-94}$$

where the random force coming from thermal fluctuation is considered as Wiener process governed by the following probability density function

$$P[f_{ran}\Delta\bar{t}] = \frac{1}{\sqrt{\frac{16k_B T \alpha \pi^4 \ell^3}{a^3} \cos^2 \left[ \frac{2\pi\ell}{a} \bar{x}(\bar{t}) \right] \Delta\bar{t}}} \exp \left\{ -\frac{(f_{ran}\Delta\bar{t})^2}{\frac{16k_B T \alpha \pi^3 \ell^3}{a^3} \cos^2 \left[ \frac{2\pi\ell}{a} \bar{x}(\bar{t}) \right] \Delta\bar{t}} \right\}. \tag{S-95}$$

Above equation can be numerical solved by forth-order Runge-Kutta method as given in Ref. [49].

## S-XII. GEOMETRY PHASE

As generalization from the concept of geometric phase introduced by Pancharatnam in classical optics and later by Berry in quantum cyclic evolution, the geometric phase of a mixed state quantum system under nonunitary evolution has been developed by Tong et al [28].

If density matrix  $\hat{\rho}_S(\bar{t})$  can be decomposed into eigenvectors  $|\phi_k(\bar{t})\rangle$  and eigenvalues  $\xi_k(\bar{t})$  as

$$\hat{\rho}_S(\bar{t}) = \sum_k \xi_k(\bar{t}) |\phi_k(\bar{t})\rangle \langle \phi_k(\bar{t})|, \tag{S-96}$$

the geometry phase is given as

$$\gamma_{phase} = \gamma(T), \tag{S-97}$$

where  $T$  is the period of evolution without dissipation while  $\gamma(\bar{t})$  is the following function

$$\gamma(\bar{t}) = \arg \left[ \sum_k \sqrt{\xi_k(0)\xi_k(\bar{t})} \langle \phi_k(0) | \phi_k(\bar{t}) \rangle \exp \left( -\int_0^{\bar{t}} \left\langle \phi_k(\bar{t}) \left| \frac{d\phi_k}{d\bar{t}}(\bar{t}) \right\rangle d\bar{t} \right) \right]. \tag{S-98}$$

In the basis  $|n^{(0)}(\bar{t})\rangle$ , the matrix representation of density matrix operator  $\hat{\rho}_S$  is given as (S-19). Then Eq. (S-96) reads

$$(\rho_S)_{n,n'}(\bar{t}) = \sum_k P_{n,k}(\bar{t}) \xi_k(\bar{t}) P_{k,n'}^\dagger(\bar{t}) \tag{S-99}$$



where  $P_{n,k}(\bar{t})$  is an unitary matrix

$$P_{n,k}(\bar{t}) = \langle n^{(0)}(\bar{t}) | \phi_k(\bar{t}) \rangle \Leftrightarrow |\phi_k(\bar{t})\rangle = \sum_n P_{n,k}(\bar{t}) |n^{(0)}(\bar{t})\rangle. \quad (\text{S-100})$$

Then the phase function is explicitly presented as

$$\gamma(\bar{t}) = \arg \left[ \sum_k \sqrt{\xi_k(0)\xi_k(\bar{t})} [P^\dagger(0)c(\bar{t})P(\bar{t})]_{kk} \exp \left( - \int_0^{\bar{t}} \left[ P^\dagger(\bar{t}) \frac{dP}{dt}(\bar{t}) - iP^\dagger(\bar{t})\sigma_t(\bar{t})P(\bar{t}) \right]_{kk} d\bar{t} \right) \right]. \quad (\text{S-101})$$

Here we use the fact that  $\langle n^{(0)}(0) | n^{(0)}(\bar{t}) \rangle = c_{n,n'}^{(0)}(\bar{t})$  and  $\langle n^{(0)}(\bar{t}) | \frac{d}{dt} n^{(0)}(\bar{t}) \rangle = -i(\sigma_t)_{n,n'}(\bar{t})$ .

### S-XIII. TUNNELING AND SLIPPING OF QUANTUM QUASI-STATIC EIGENSTATES AND CLASSICAL TRAJECTORY

According to classical mechanics, if driving the particle with a very small driving velocity  $\bar{v}$ , our particle keeps staying at the first local minimum of the potential surface i.e.  $\bar{x}(\bar{t}) \approx \bar{x}_{min,1}(\bar{t})$ . Since the minimum obeys  $\frac{\partial V(\bar{x},\bar{t})}{\partial \bar{t}} = 0$ , we find that

$$\bar{x} - \bar{v}\bar{t} + \frac{u_0}{2} \left( \frac{2\pi\ell}{a} \right) \sin \left( \frac{2\pi\ell}{a} \bar{x} \right) \approx 0 \Leftrightarrow F_L \approx \frac{\pi U_0}{a} \left( \frac{2\pi\ell}{a} \right)^2 \sin \left( \frac{2\pi\ell}{a} \bar{x} \right) \leq \frac{\pi U_0}{a}, \quad (\text{S-102})$$

which yields to the maximal lateral force at classical limit  $(F_L)_{max} = \frac{\pi U_0}{a}$  as given in Refs. [29, 45]. Correspondingly, the lateral force reaches its maximum when  $\bar{x} = \frac{a}{4\ell}$  from which we can determine the slipping time

$$\frac{a}{4\ell} - \bar{v}t_{slip,cl} + \frac{u_0}{2} \left( \frac{2\pi\ell}{a} \right) \approx 0 \Rightarrow \frac{t_{slip,cl}}{T} \approx \frac{1}{4} + \frac{u_0}{4\pi} \left( \frac{2\pi\ell}{a} \right)^2 \approx \frac{1}{4} + \frac{\eta}{2\pi}. \quad (\text{S-103})$$

Since above examination based on the assumption that our particle keeps staying at the first local minimum of the potential surface i.e.  $\bar{x}(\bar{t}) \approx \bar{x}_{min,1}(\bar{t})$ , it is only valid for small enough driving velocity  $\bar{v}$ .

Next, in order to examine the slipping time of quantum trajectory, we try to extract the slipping time associated to each quasi-static eigenstate  $t_{slip,n}$ . For each quasi-static eigenstate  $|n(\bar{t})\rangle$ , we evaluate the statistical average of relative displacement between the particle and the center of the harmonic trap  $\langle \bar{x}_n \rangle - \bar{v}\bar{t}$  within the first period. Results for the first 5 eigenstates  $n = 0, 1, 2, 3, 4$  are given in Figs. S-3(a,b,c,d,e). The slipping time of each quasi-static eigenstate  $t_{slip,n}$  is then determined as the moment when  $\langle \bar{x}_n \rangle - \bar{v}\bar{t}$  reaches its minimum (circled) and  $t_{slip,n}$  should be in the period when the potential surface forms a double-well shape ( $0.32T \leq t \leq 0.68T$ ). Our calculation finds that  $t_{slip,n=0} = 0.485T$  (Fig. S-3(a,g)),  $t_{slip,n=1} = 0.519T$  (Fig. S-3(b,i)),  $t_{slip,n=2} = 0.578T$  (Fig. S-3(c,k)) while there are no slipping time corresponding to the higher quasi-static eigenstates. Furthermore, Figs. S-3(f,g,h,i,j,k,l,m,n) illustrate how eigenstates wavefunction and potential surface look like at different moments of time including slipping time of the first 3 eigenstates and the tunneling time between these states as well as the classical slipping time.

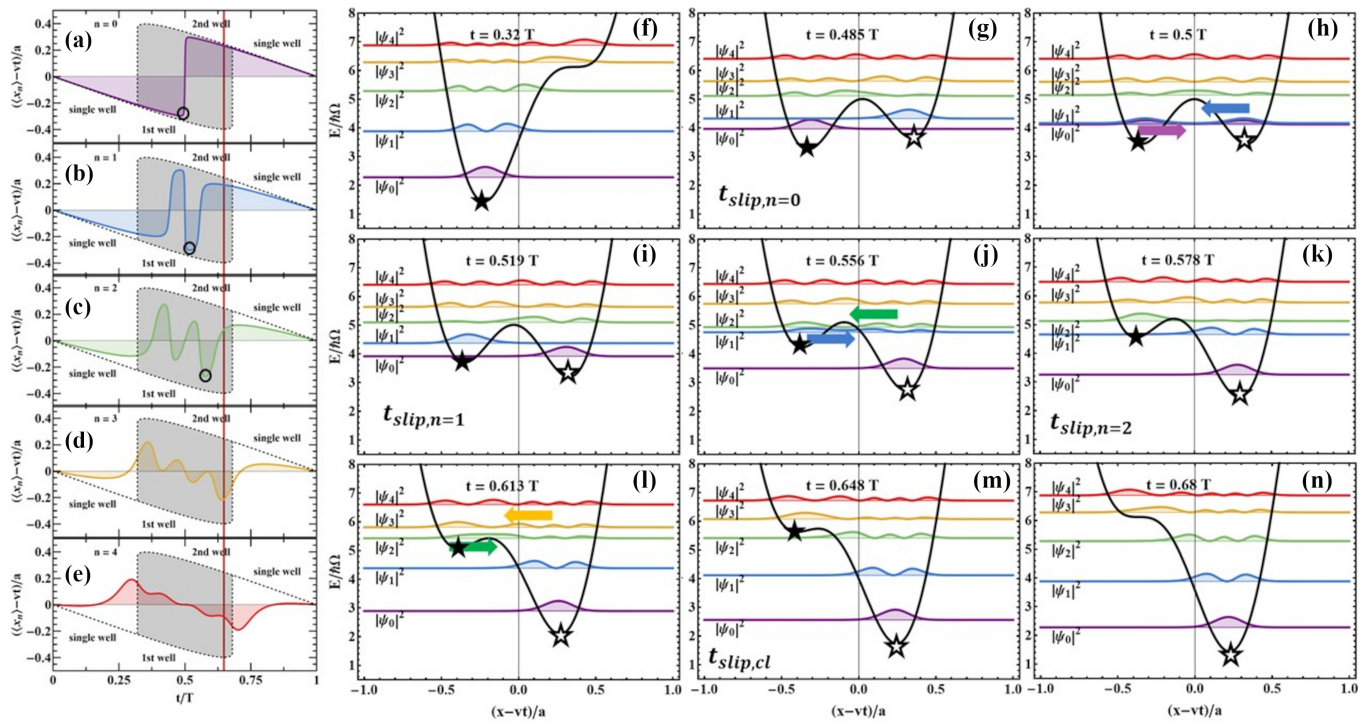


FIG. S-3. (a,b,c,d,e) The statistical average of relative displacement between the particle and the center of the harmonic trap  $\langle \bar{x}_n \rangle - \bar{v}t$  within the first period for  $n = 0, 1, 2, 3, 4$ . For comparison purpose, black curves are for minimums of potential surface of the particle. The vertical grid line associates to the classical slipping time  $t_{slip,cl} \approx 0.648T$ . (f,g,h,i,j,k,l,m,n) Potential surface, quasi-static eigenvalues and associated modulus-squared eigenstates for the first 5 states when the potential surface forms a double-well shape ( $t = 0.32 - 0.68T$ ).

## S-XIV. ANIMATION OF QUANTUM AND CLASSICAL MOTIONS

FIG. S-4. Dynamical animation (GIF) describes quantum and classical motions of the particle driven by a harmonic trap with a velocity of  $v = 0.005\nu$  along a one-dimensional chain. The total potential surface (solid red) and harmonic potential trap (dashed green), total energy (purple) of the particle are also shown. Besides, the heat released to the surrounding environment is normalized by its maximal classical value in both quantum and classical motions. In quantum motion, the population distribution on quasi-state eigenstates is also given at each point of time.

- 
- [1] A. I. Volokitin and B. N. J. Persson, Near-field radiative heat transfer and noncontact friction, *Rev. Mod. Phys.* **79**, 1291 (2007).
  - [2] A. Vakis, V. Yastrebov, J. Scheibert, L. Nicola, D. Dini, C. Minfray, A. Almqvist, M. Paggi, S. Lee, G. Limbert, J. Molinari, G. Anciaux, R. Aghababaei, S. Echeverri Restrepo, A. Papangelo, A. Cammarata, P. Nicolini, C. Putignano, G. Carbone, S. Stupkiewicz, J. Lengiewicz, G. Costagliola, F. Bosia, R. Guarino, N. Pugno, M. Müser, and M. Ciavarella, Modeling and simulation in tribology across scales: An overview, *Tribol. Int.* **125**, 169 (2018).
  - [3] M. Wolloch, G. Losi, M. Ferrario, and M. C. Righi, High-throughput screening of the static friction and ideal cleavage strength of solid interfaces, *Sci. Rep.* **9**, 17062 (2019).
  - [4] S. Cahangirov, C. Ataca, M. Topsakal, H. Sahin, and S. Ciraci, Frictional Figures of Merit for Single Layered Nanostructures, *Phys. Rev. Lett.* **108**, 126103 (2012).
  - [5] R. K. Barik and L. M. Woods, Frictional Properties of Two-Dimensional Materials: Data-Driven Machine Learning Predictive Modeling, *ACS Applied Materials & Interfaces* **16**, 40149 (2024), <https://doi.org/10.1021/acsami.4c05532>.
  - [6] M. Wolloch, G. Levita, P. Restuccia, and M. C. Righi, Interfacial Charge Density and Its Connection to Adhesion and Frictional Forces, *Phys. Rev. Lett.* **121**, 026804 (2018).

- [7] P. C. Torche, A. Silva, D. Kramer, T. Polcar, and O. Hovorka, Multi-scale model predicting friction of crystalline materials, *Adv. Mater. Interfaces* **9**, 2100914 (2022).
- [8] I. Szlufarska, M. Chandross, and R. W. Carpick, Recent advances in single-asperity nanotribology, *J. Phys. D: Appl. Phys.* **41**, 123001 (2008).
- [9] G. Tomlinson, CVI. A molecular theory of friction, *London Edinb. Dublin Philos. Mag. J. Sci.* **7**, 905 (1929).
- [10] L. Prandtl, Ein Gedankenmodell zur kinetischen Theorie der festen Körper, *J. Appl. Math. Mech.* **8**, 85 (1928).
- [11] F. R. Krajewski and M. H. Müser, Quantum Creep and Quantum-Creep Transitions in 1D Sine-Gordon Chains, *Phys. Rev. Lett.* **92**, 030601 (2004).
- [12] F. R. Krajewski and M. H. Müser, Quantum dynamics in the highly discrete, commensurate Frenkel Kontorova model: A path-integral molecular dynamics study, *J. Chem. Phys.* **122**, 124711 (2005).
- [13] H. Xu, W. Chen, and Y. Zhu, Influence of the bond defect in driven Frenkel-Kontorova chains, *Phys. Rev. B* **75**, 224303 (2007).
- [14] L. Landau, Zur Theorie der Energieübertragung. II, *Physikalische Zeitschrift der Sowjetunion* **2**, 46–51 (1932).
- [15] C. Zener, Non-Adiabatic Crossing of Energy Levels, *Proc. R. Soc. London Ser. A* **137**, 696 (1932).
- [16] V. L. Pokrovsky and N. A. Sinitsyn, Landau-Zener transitions in a linear chain, *Phys. Rev. B* **65**, 153105 (2002).
- [17] Z. Huang and Y. Zhao, Dynamics of dissipative Landau-Zener transitions, *Phys. Rev. A* **97**, 013803 (2018).
- [18] T. Zanca, F. Pellegrini, G. E. Santoro, and E. Tosatti, Frictional lubricity enhanced by quantum mechanics, *Proc. Natl. Acad. Sci. U.S.A.* **115**, 3547 (2018).
- [19] L. Arceci, S. Barbarino, R. Fazio, and G. E. Santoro, Dissipative Landau-Zener problem and thermally assisted Quantum Annealing, *Phys. Rev. B* **96**, 054301 (2017).
- [20] A. Stone, *The Theory of Intermolecular Forces* (Oxford University Press, 2013).
- [21] See Supplementary Information for detail derivations of coupling potential between the nanoparticle and the atomic chain, matrix elements of quantum Prandtl-Tomlinson Hamiltonian in moving harmonic oscillator basis set, numerical calculation for quasi-static eigenenergies and eigenstates, quantum evolution with and without external bath reservoir, classical evolution with and without external bath reservoir; detail explanations for tunneling and slipping of quantum and classical trajectories and an animation (GIF) of quantum and classical motions; see also Refs. [48, 49] therein.
- [22] E. Meyer, T. Gyalog, R. M. Overney, and K. Dransfeld, *Nanoscience: Friction and Rheology on the Nanometer Scale* (World Scientific, 1998).
- [23] M. H. Müser, Velocity dependence of kinetic friction in the Prandtl-Tomlinson model, *Phys. Rev. B* **84**, 125419 (2011).
- [24] J. J. Sakurai and J. Napolitano, *Modern Quantum Mechanics*, 3rd ed. (Cambridge University Press, 2020).
- [25] M. Yamaguchi, T. Yuge, and T. Ogawa, Markovian quantum master equation beyond adiabatic regime, *Phys. Rev. E* **95**, 012136 (2017).
- [26] The considered time domain for the moving particle (from  $t_{min} = 0$  to  $t_{max} = 3T$  in this study) is divided evenly by infinitesimal small intervals  $\Delta t$  who must be smaller than the smallest period of Bohr oscillation between eigenstates  $\Delta t < |\max(E_n(\bar{t}) - E_m(\bar{t}))|^{-1}$ .
- [27] N. A. Peters, T.-C. Wei, and P. G. Kwiat, Mixed-state sensitivity of several quantum-information benchmarks, *Phys. Rev. A* **70**, 052309 (2004).
- [28] D. M. Tong, E. Sjöqvist, L. C. Kwek, and C. H. Oh, Kinematic Approach to the Mixed State Geometric Phase in Nonunitary Evolution, *Phys. Rev. Lett.* **93**, 080405 (2004).
- [29] A. Socoliuc, R. Bennewitz, E. Gnecco, and E. Meyer, Transition from Stick-Slip to Continuous Sliding in Atomic Friction: Entering a New Regime of Ultralow Friction, *Phys. Rev. Lett.* **92**, 134301 (2004).
- [30] D. Gangloff, A. Bylinskii, I. Counts, W. Jhe, and V. Vuletić, Velocity tuning of friction with two trapped atoms, *Nat. Phys.* **11**, 915–919 (2015).
- [31] I. Counts, D. Gangloff, A. Bylinskii, J. Hur, R. Islam, and V. Vuletić, Multislip Friction with a Single Ion, *Phys. Rev. Lett.* **119**, 043601 (2017).
- [32] D.-N. Le, N.-T. D. Hoang, and V.-H. Le, Exact analytical solutions of the schrödinger equation for a two dimensional purely sextic double-well potential, *Journal of Mathematical Physics* **59**, 032101 (2018), <https://doi.org/10.1063/1.4997532>.
- [33] A. O. Caldeira and A. J. Leggett, Influence of Dissipation on Quantum Tunneling in Macroscopic Systems, *Phys. Rev. Lett.* **46**, 211 (1981).
- [34] U. Weiss, *Quantum Dissipative Systems*, 4th ed. (World Scientific, Singapore, 2012).
- [35] T. Dittrich, P. Hänggi, G.-L. Ingold, B. Krammer, G. Schön, and W. Zwerger, *Quantum transport and dissipation* (Wiley-VCH, Weinheim, Germany, 1998).
- [36] S. Shevchenko, S. Ashhab, and F. Nori, Landau–zener–stückelberg interferometry, *Physics Reports* **492**, 1 (2010).
- [37] D. Bouwmeester, G. P. Karman, C. A. Schrama, and J. P. Woerdman, Observation of interference in transitions due to local geometric phases, *Phys. Rev. A* **53**, 985 (1996).
- [38] S. Gasparinetti, P. Solinas, and J. P. Pekola, Geometric landau-zener interferometry, *Phys. Rev. Lett.* **107**, 207002 (2011).
- [39] L. Viotti, F. C. Lombardo, and P. I. Villar, Geometric phase in a dissipative jaynes-cummings model: Theoretical explanation for resonance robustness, *Phys. Rev. A* **105**, 022218 (2022).
- [40] F. C. Lombardo and P. I. Villar, Geometric phases in open systems: A model to study how they are corrected by decoherence, *Phys. Rev. A* **74**, 042311 (2006).
- [41] L. Viotti, A. L. Gramajo, P. I. Villar, F. C. Lombardo, and R. Fazio, Geometric phases along quantum trajectories, *Quantum* **7**, 1029 (2023).
- [42] S. M. Rytov, Y. A. Kravtsov, and V. I. Tatarskii, *Principles of Statistical Radiophysics 3* (Springer, Berlin, Germany,

- 1989).
- [43] C.-W. Yang, K.-t. Leung, R.-F. Ding, H.-C. Ko, Y.-H. Lu, C.-K. Fang, and I.-S. Hwang, Lateral force microscopy of interfacial nanobubbles: Friction reduction and novel frictional behavior, [Scientific Reports](#) **8**, 3125 (2018).
  - [44] E. Schäffer, S. F. Nørrelykke, and J. Howard, Surface forces and drag coefficients of microspheres near a plane surface measured with optical tweezers, [Langmuir](#) **23**, 3654 (2007).
  - [45] E. Gnecco, R. Roth, and A. Baratoff, Analytical expressions for the kinetic friction in the Prandtl-Tomlinson model, [Phys. Rev. B](#) **86**, 035443 (2012).
  - [46] E. Bonvin, L. Devaud, M. Rossi, A. Militaru, L. Dania, D. S. Bykov, M. Teller, T. E. Northup, L. Novotny, and M. Frimmer, Hybrid paul-optical trap with large optical access for levitated optomechanics, [Phys. Rev. Res.](#) **6**, 043129 (2024).
  - [47] A. Zenesini, H. Lignier, G. Tayebirad, J. Radogostowicz, D. Ciampini, R. Mannella, S. Wimberger, O. Morsch, and E. Arimondo, Time-resolved measurement of landau-zener tunneling in periodic potentials, [Phys. Rev. Lett.](#) **103**, 090403 (2009).
  - [48] I. S. Gradshteyn and I. M. Ryzhik, *Table of integrals, series, and products* (Academic press, 2014).
  - [49] J. Wilkie and M. Çetinbaş, Variable-stepsize runge–kutta methods for stochastic schrödinger equations, [Physics Letters A](#) **337**, 166 (2005).